

Annual Review of Marine Science

Modeling the Morphodynamics of Coastal Responses to Extreme Events: What Shape Are We In?

Christopher R. Sherwood,¹ Ap van Dongeren,^{2,3} James Doyle,⁴ Christie A. Hegermiller,¹ Tian-Jian Hsu,⁵ Tarandeep S. Kalra,⁶ Maitane Olabarrieta,⁷ Allison M. Penko,⁸ Yashar Rafati,⁵ Dano Roelvink,^{2,3,9} Marlies van der Lugt,^{2,9} Jay Veeramony,⁸ and John C. Warner¹

¹Woods Hole Coastal and Marine Science Center, US Geological Survey, Woods Hole, Massachusetts 02543, USA; email: csherwood@usgs.gov

²Marine and Coastal Systems, Deltares, 2629 HV Delft, The Netherlands

³Coastal and Urban Risk and Resilience, IHE Delft Institute for Water Education, 2611 AX Delft, The Netherlands

⁴US Naval Research Laboratory, Monterey, California 93943, USA

⁵Center for Applied Coastal Research, Department of Civil and Environmental Engineering, University of Delaware, Newark, Delaware 19716, USA

⁶Integrated Statistics (contracted to the US Geological Survey), Woods Hole, Massachusetts 02543, USA

⁷Department of Civil and Coastal Engineering, University of Florida, Gainesville, Florida 32611, USA

⁸US Naval Research Laboratory, Stennis Space Center, Mississippi 39529, USA

⁹Faculty of Civil Engineering and Geosciences, Delft University of Technology, 2628 CD Delft, The Netherlands

**ANNUAL
REVIEWS CONNECT**

www.annualreviews.org

- Download figures
- Navigate cited references
- Keyword search
- Explore related articles
- Share via email or social media

Annu. Rev. Mar. Sci. 2022. 14:457–92

First published as a Review in Advance on July 27, 2021

The *Annual Review of Marine Science* is online at marine.annualreviews.org

<https://doi.org/10.1146/annurev-marine-032221-090215>

This is a work of the US government and not subject to copyright protection in the United States

Keywords

coastal morphodynamics, extreme storms, coastal modeling, sandy coasts, waves, sediment transport

Abstract

This review focuses on recent advances in process-based numerical models of the impact of extreme storms on sandy coasts. Driven by larger-scale models of meteorology and hydrodynamics, these models simulate morphodynamics across the Sallenger storm-impact scale, including swash,

collision, overwash, and inundation. Models are becoming both wider (as more processes are added) and deeper (as detailed physics replaces earlier parameterizations). Algorithms for wave-induced flows and sediment transport under shoaling waves are among the recent developments. Community and open-source models have become the norm. Observations of initial conditions (topography, land cover, and sediment characteristics) have become more detailed, and improvements in tropical cyclone and wave models provide forcing (winds, waves, surge, and upland flow) that is better resolved and more accurate, yielding commensurate improvements in model skill. We foresee that future storm-impact models will increasingly resolve individual waves, apply data assimilation, and be used in ensemble modeling modes to predict uncertainties.

1. INTRODUCTION

This review discusses advances in modeling coastal morphology changes caused by extreme storms such as tropical cyclones and extratropical storms, with an emphasis on the morphological change of sandy beaches and barrier islands. We focus on process-based models that are quantitative representations of our understanding of coastal hydrodynamics, sediment transport, and morphological change and that are intended to hindcast and/or forecast processes on the temporal and spatial scales of extreme storms. These events produce the fastest and most severe natural morphological changes that shape the coastal landscape, define habitats, and present risks to humans and infrastructure.

Our review draws on experience gained during the Increasing the Fidelity of Morphological Storm Impact Predictions (IFMSIP) project, funded by the US Office of Naval Research and executed by a consortium of scientists from the US Geological Survey, US Naval Research Laboratory, University of Florida, University of Delaware, and IHE Delft Institute for Water Education, coordinated by Deltares in the Netherlands. The aim of the project was to utilize advances in process knowledge, data-acquisition techniques, and computing power to (a) better understand the accuracy of morphodynamic numerical model results compared with observational data when applied to extreme storms, (b) improve the accuracy of event-driven morphological predictions, (c) improve predictions by improving parameter estimates and identifying key processes and sensitivities to inputs, and (d) improve confidence in model applications in new environments.

The extent of morphological change during a coastal storm, including dune/beach erosion, overwash, and breach/inlet formation, has been related to a storm-impact scale proposed by Sallenger (2000). Sallenger's four impact regimes depend on the maximum total water level relative to the dune morphology. This simple scale provides an initial estimate of the impact severity but masks the complexity of the hydrodynamic and sediment-transport processes and feedbacks that drive the changes. Models must be capable of representing change across all stages of the Sallenger scale, so our discussion of modeled processes takes this perspective.

Recent reviews related to morphodynamic modeling (de Swart & Zimmerman 2009, Coco et al. 2013) focused on the evolution of coastal and fluvial systems at temporal scales longer than those corresponding to individual storms. No recent reviews have directly addressed the coastal response to extreme storms, where changes are a short-term (~hours–days) response to intense forcing, rather than a long-term evolution of a self-organized system.

A 2016 review of the modeling of river morphodynamics (Siviglia & Crosato 2016) revealed four recent trends: (a) the adoption of open-source and often community-developed codes; (b) the tendency for simulations to be performed on ever-larger domains, often with mixed grain sizes; (c) the expansion of morphological evolution beyond bathymetry, to include subaerial morphological changes such as bank erosion, braiding, and vegetation effects; and (d) the development of

new numerical schemes. The authors also concluded that the many complicating factors (such as roughness and sediment-transport formulae and forecasting of future hydrographs) lead to large uncertainties and that the interpretation of model results depends strongly on the experience and expertise of the modelers. Similar trends are recognized in coastal modeling, as detailed below.

Our review focuses on process-based modeling of the response of the coastal morphology to extreme storms. Although our examples are drawn mostly from tropical storms, the processes discussed apply to most storms accompanied by large waves and elevated water levels. We limit our review to open sandy coasts, including barrier islands, which constitute 31% of the world's coasts (Luijendijk et al. 2018). We discuss the hydrodynamic impacts of water levels and waves on the coastal zone. To properly represent the far-field hydrodynamics that ultimately force local change, numerical models with domains of hundreds of kilometers and resolutions of hundreds of meters are required. These fields of driving forces are nested down to compute the morphodynamic impact at local scales with $O(1)$ -m resolution, which (with current computational resources) limits the extent of the morphological domain to $O(10)$ km. We assess the state of our understanding of essential processes, highlight particularly important developments, and touch on ongoing trends in modeling.

In Section 2, we introduce the types of models used to simulate coastal morphodynamic change and relate the processes included in these models to the Sallenger scale. Section 3 describes modeling approaches to key coastal processes, and Section 4 discusses model skill. Finally, in Section 5, we evaluate progress on particularly problematic processes and identify trends in coastal modeling.

2. PROCESS-BASED MODELS OF COASTAL STORM MORPHODYNAMICS

We describe in this section the types of process-based models that are suitable for simulating morphological impacts classified using the Sallenger (2000) scale. We describe the dominant forcing and response in each regime and implications for modeling.

2.1. Types of Models

Roelvink & Reniers (2012) divided coastal morphology models into three types, based primarily on dimensionality: (a) one-dimensional (1D) cross-shore profile models (Bruun 1954, 1962; Roelvink & Brøker 1993; Schoonees & Theron 1995), including equilibrium shoreline models (Miller & Dean 2004; Yates et al. 2009, 2011); (b) 1D alongshore coastline models (Pelnard-Considère 1957; Dean 1991; Larson et al. 1997; Ashton et al. 2001; Buijsman et al. 2001; Ashton & Murray 2006; Davidson et al. 2010, 2013; Splinter et al. 2014; Vitousek et al. 2017); and (c) two-dimensional (2D) and three-dimensional (3D) models (de Vriend et al. 1993, Nicholson et al. 1997). Vitousek et al. (2017) distinguished between physics-based and process-based models. In their vernacular, physics-based models solve conservation equations for the mass and momentum of water and sediment and attempt to treat all the processes important to coastal evolution, whereas process-based models focus on a single dominant phenomenon. In this review, we equate physics-based models with Vitousek et al.'s (2017) definition of process-based models and note that all models rely on empiricism at some scale. Examples of models describing phenomena include those by Bruun (1962), Yates et al. (2009), and Long & Plant (2012). These models typically parameterize unresolved physics and use observations to optimize the model parameters with techniques ranging from a simple least squares fit to Kalman filtering. Hence, these models may apply only to specific locations but have proved useful for the study of seasonal and long-term morphological changes. Examples of (2D and 3D) process-based models include Delft3D (Roelvink & van Banning 1995,

Lesser et al. 2004), XBeach (Roelvink et al. 2009), MIKE 21 (Warren & Bach 1992, Kaergaard & Fredsoe 2013), NearCoM-TVD (Chen et al. 2014), FVCOM (Chen et al. 2003, Lai et al. 2010, Wu et al. 2011), TELEMAC-MASCARET (<http://www.opentelemac.org>) (Hervouet 2007, Davies & Robins 2017, Kaveh et al. 2019) and the accompanying sediment and morphology module SISYPHE (Tassi & Villaret 2014), TK-2D software (Li et al. 2020), BASEMENT (Vetsch et al. 2014), ECOMSED (Han & Huang 2018), and COAWST (Warner et al. 2008b, 2010). These models represent processes through equations that conserve mass and momentum but often parameterize small-scale processes. Many of these models were described and compared by Amoudry & Souza (2011).

Murray (2003) suggested that models can be arranged in three ways: (a) simulation versus exploration, (b) bottom up versus top down (scale), and (c) equation based versus rules based. Process-based models are what Murray (2003) would call “explicit numerical reductionism” (p. 152), in that they attempt to start bottom up by representing processes at the smallest and fastest scales feasible and then integrate those results temporally and spatially to produce results at useful scales (Coco et al. 2013). As model integrations are upscaled, uncertainties and biases accumulate, possibly rendering the results so uncertain as to be meaningless. This is especially a concern for long-term (years or more) simulations of self-organized systems but may be less of a concern for event-scale simulations, especially if these models are well calibrated against laboratory and field data of past events. The alternatives are top-down exploratory models that simplify the models by abstraction, including only the most important factors relevant to the process at hand (Murray 2003, 2007; Coco et al. 2013). These types of models have proven useful in isolating and demonstrating the dominance of key processes in certain environments, such as the effect of wave angle on the development of alongshore features (Ashton & Murray 2006), the role of roughness in the formation of rippled scour depressions (Murray & Thielert 2004), and the importance of fetch and vegetation in dune formation (Durán & Moore 2013). However, because top-down models lack a full suite of fundamental physics, they are restricted to special cases. Therefore, despite the potential drawbacks outlined above, bottom-up, process-based models are the most applicable types for computing coastal morphological change in complex environments and are therefore the focus of this review.

2.2. Sallenger Regimes

The Sallenger (2000) scale (**Figure 1**) provides a framework for discussing the most important physical processes and their morphodynamic agency across the shoreface, beach, and backshore during morphologically significant storm events. Process-based models should include physics or parameterizations to simulate processes across all Sallenger regimes, but not all physical processes are dominant in every regime.

In the swash regime, incident-band (2–25-s periods) and infragravity (25–250-s periods) waves run up the beach but do not reach the dune toe. Morphological changes are relatively minor and confined to the subaqueous nearshore and the upper shoreface, despite strong motions and transports. Dominant morphodynamic processes in the swash regime include swash-induced transport modulated by infragravity motions, longshore transport by wave-driven currents, and cross-shore transport driven by wave asymmetry and undertow.

Beach profiles can either erode or accrete during swash conditions, and surf-zone bars can migrate onshore or offshore, depending on the balance of onshore sediment transport driven by asymmetry in wave-orbital velocity or acceleration and offshore transport by undertow or rip currents (e.g., Gallagher et al. 1998, Hoefel & Elgar 2003, Hsu et al. 2006, Fernández-Mora et al. 2015). Whether berms accrete and the shoreline advances may depend on the value of the

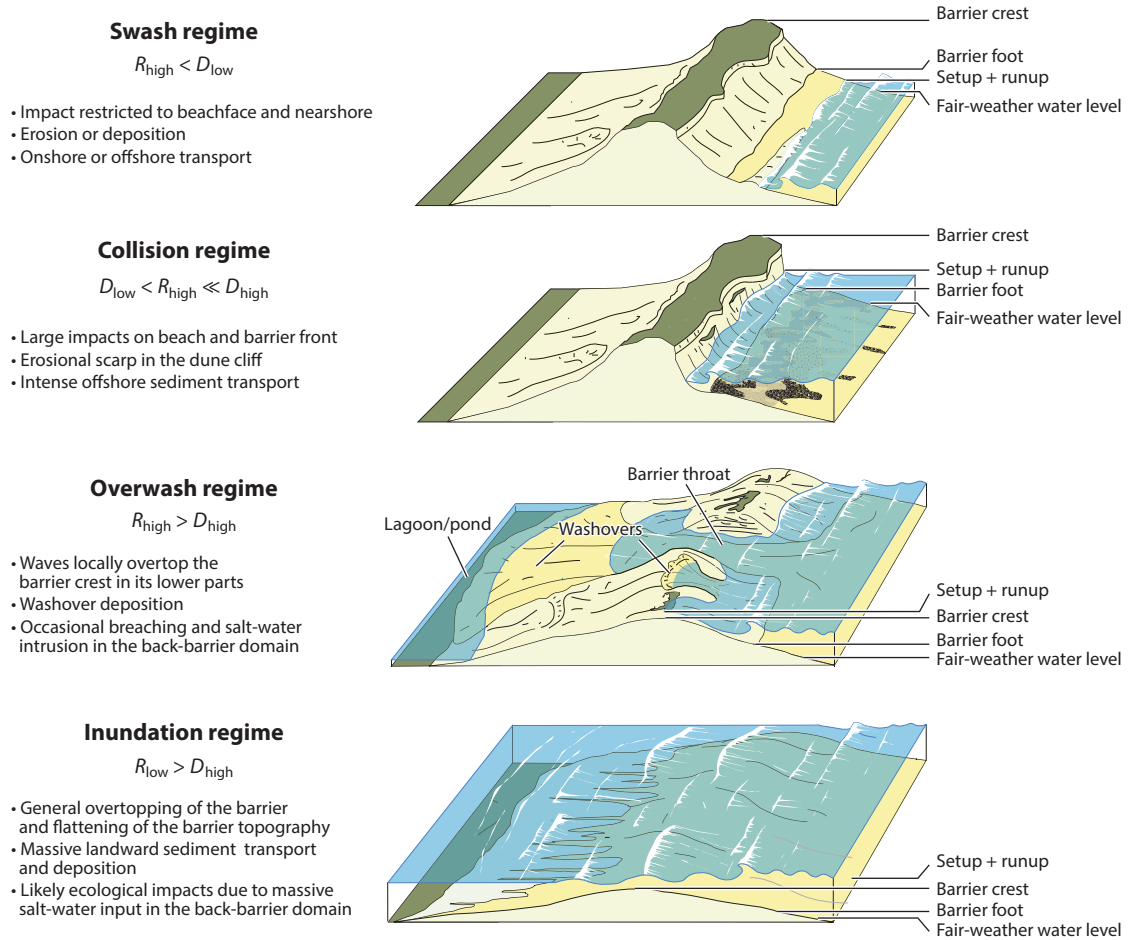


Figure 1

The Sallenger (2000) storm-impact scale. D_{high} denotes the height of the barrier crest, D_{low} denotes the height of the barrier foot, R_{high} denotes the highest action of the waves (tide + surge + setup + runup), and R_{low} denotes the lowest action of the waves (tide + surge + setup). Figure adapted with permission from Goslin & Clemmensen (2017); copyright 2017 Elsevier.

dimensionless fall velocity (Gorlay 1968) relative to some long-term equilibrium value, which is the basis of some shoreline models (e.g., Miller & Dean 2004, Davidson et al. 2013, Splinter et al. 2014, Montañó et al. 2020).

Models of the swash zone should include the physics of wave refraction and transformation, including wave breaking, wave-driven undertow and longshore currents, and wave- and current-driven bedload and suspended sediment transport. While many models have incorporated these processes, some struggle to correctly represent swash behavior on the upper shoreface, creating scarps where this should not happen (e.g., Vousdoukas et al. 2012), especially when the beach slope is relatively steep. The reason is that transport across the instantaneous water line is not well resolved, and heuristic approaches to controlling the morphology of the foreshore beach slope (as in Roelvink & Costas 2019 and Roelvink et al. 2019) are required to prevent unrealistic behavior that eventually affects the whole profile.

In the collision regime, swash consisting of incident and infragravity waves strikes the dune face (van Thiel de Vries et al. 2008), releasing volumes of sand onto the beach, where it is within reach of flows that can transport the sand alongshore or offshore. Models must represent incident and infragravity waves, as the former are modulated by the latter with a significant effect on the dune erosion process (e.g., van Thiel de Vries et al. 2008). Models must also incorporate the slumping of sand from the dune face. Key transport processes in the collision regime are the same as those for the swash regime, plus dune erosion and dune slumping.

In the overwash regime, waves occasionally reach and overtop the dune or berm, as their height and runup are modulated by infragravity waves with amplitudes of a half meter or more (see summaries in Bertin et al. 2018 and Billson et al. 2019). A subtle interplay of runup and backwash processes may determine whether they lead to increased or decreased berm elevations. On longer timescales, sediment transported offshore during collision can be returned during recovery of the beach and dune, but overwash processes are less reversible and lead to barrier transgression. All the processes listed above continue to be relevant in the overwash regime.

The inundation regime occurs when steady wave setup and surge exceed the dune or berm elevation and water flows over the crest. Sallenger (2000) assigned this regime the highest potential for morphological change. Inundation is associated with significant onshore transport and causes erosion and breaching. Cross-shore transport during inundation can occur as open-channel flow and can be affected by flow impedance from vegetation and structures. Wave processes are less dominant in this case, as the morphological development is dominated by current-induced sediment transport and the slumping of sand into the newly formed breach (Visser 1994).

One common process that Sallenger (2000) did not include is seaward-directed flow, or outwash (Over et al. 2021; see figure 7 in Harter & Figlus 2017), which can occur when back-barrier water levels exceed those on the ocean side. Storm surge can inundate marshes or flood back-barrier lagoons. As forcing relaxes, this water returns seaward (Lennon 1991, Goff et al. 2010, Harter & Figlus 2017, Goff et al. 2019, Over et al. 2021) and can scour new breaches or deepen existing channels. Alternatively, winds blowing across back-barrier sounds can generate surge along the backside of barrier islands. This can result in significant seaward transport of sand and aid in the establishment of new inlets. Although the ultimate stability of new inlets may depend on the general setting of the barrier, back bay, and other inlets (e.g., van Ormondt et al. 2020), the initial channel deepening by ebb-return scouring may be a decisive process in inlet formation. For models to resolve this seaward-flow regime, they must include the dynamics of back-barrier water levels.

3. METEOROLOGICAL FORCING, HYDRODYNAMIC, AND MORPHODYNAMIC PROCESSES

3.1. Meteorology

The demand for more accurate forecasts of the tracks of tropical cyclones, as well as their intensity and wind distribution (or structure), with greater lead times is higher than ever due to the large economic and societal impacts of these storms. A noteworthy example occurred during October 2012, when Hurricane Sandy threatened many communities along the US East Coast. The path and intensity of Sandy had profound implications for the surge and inundation that would ultimately impact the millions of people and billions of dollars of vulnerable assets in its path. With an estimated total damage amount of US\$70 billion or more, Sandy was one of the costliest storms in US history and the deadliest to hit the northeast United States in four decades (Blake et al. 2013).

One of the challenges with the prediction of tropical cyclones is that the important processes are inherently multiscale in nature. The tracks of tropical cyclones depend primarily on the steering flow arising from the larger-scale environment (e.g., Marks & Shay 1998), such as synoptic- and mesoscale tropical and extratropical troughs and ridges, closed lows, tropical upper-tropospheric troughs, monsoon troughs, and gyres. The processes governing the intensity and size of tropical cyclones depend on both the inner-core dynamics and the larger-scale environment (e.g., Braun et al. 2006, Rogers et al. 2006), as well as on air–sea interaction processes (e.g., Black et al. 2007, Fairall et al. 2009, D’Asaro et al. 2011). This motivates the requirement for accurate representation in models of the key physical and dynamical processes within the storm itself and in the larger-scale environment.

Key processes governing tropical cyclone structure (pressure and wind fields) and intensification include diabatic heating associated with atmospheric convection, particularly in the eye-wall region, as well as boundary-layer processes, including air–sea interaction. High-resolution models have been increasingly applied to capture these processes and resolve the critically important inner part of the storm, which includes the eye, eye wall, and spiral rainbands (e.g., Davis et al. 2008). The Coupled Boundary Layers Air–Sea Transfer (CBLAST) field program (Black et al. 2007) provided important air–sea interaction observations in hurricanes and motivated new approaches to the parameterization of these processes in tropical cyclone models. Coupled air–ocean and air–ocean–wave tropical cyclone modeling systems represent these key air–sea interaction processes in closer agreement with observations than noncoupled models (e.g., Bao et al. 2000, Chen et al. 2010, Olabarrieta et al. 2012, Zambon et al. 2014).

3.2. Improvement of Meteorological Forcing

The remarkable improvement of tropical cyclone track prediction (e.g., Goerss 2007, Hamill et al. 2011) (**Figure 2a**) has been fueled in part by more skillful global prediction models (Bauer et al. 2015). Improvements can be attributed to more sophisticated data-assimilation systems that take advantage of many more satellite-based observations and more realistic representations of physical processes or physical parameterizations of the boundary layer, clouds, radiative forcing, precipitation, land surface, and ocean–atmosphere interactions (Bauer et al. 2015). A three-day hurricane track forecast today is as skillful as a one-day forecast was 30 years ago. The costs of evacuating coastal areas before a hurricane are substantial—broadly estimated to be US\$1.4 million (adjusted) for every mile of coastline evacuated (e.g., Whitehead 2003). The improved track forecasts have steadily reduced the sizes of evacuation areas and mitigated costs. However, there has been less emphasis on evaluating the skill of accurately predicting tropical cyclone translation speeds, which is important for hydro- and morphodynamic models.

The prediction of tropical cyclone intensity and structure remains a challenge, and considerable progress has been made in the last decade, but not as quickly as the track forecast improvements (e.g., DeMaria et al. 2005, Rogers et al. 2006) (**Figure 2b**). The slower improvement in forecasts of tropical cyclone intensity and structure can be attributed to a lack of critical observations in the tropical cyclone inner core and the surrounding environment and inaccurate representations of physical processes in numerical weather prediction models. It has been hypothesized that track-prediction skill depends more on large-scale processes (e.g., Marks & Shay 1998), while intensity-prediction skill depends on both the inner-core dynamics and their relationship to the environment (e.g., Braun et al. 2006, Rogers et al. 2006), as well as air–sea interaction processes (e.g., Black et al. 2007, Fairall et al. 2009, D’Asaro et al. 2011). Tropical cyclone intensity for strong tropical cyclones is correlated with translation speed, which is associated with upper-ocean effects (e.g., Mei et al. 2012).

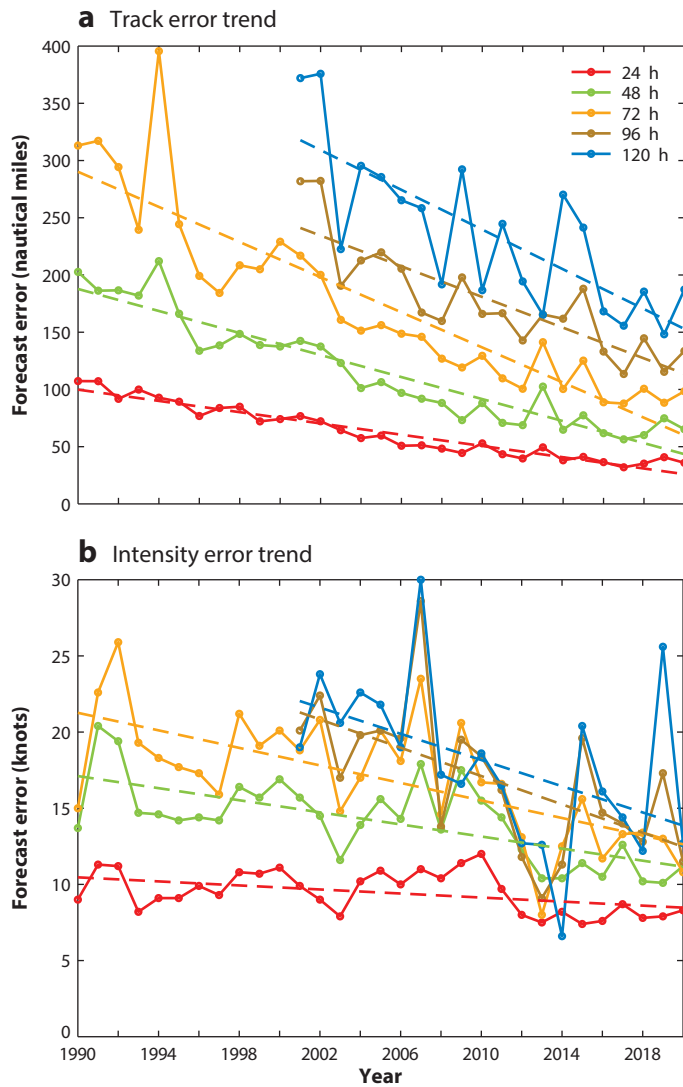


Figure 2

Time series of (a) hurricane track error and (b) hurricane intensity error in the Atlantic basin, showing the error trends decreasing with time. Figure adapted from Natl. Hurric. Cent. (2020).

It remains a challenge for current operational models to predict tropical cyclone tracks and intensities with enough fidelity and accuracy to provide forcing for real-time surge and inundation models. The averaged track errors from five-day forecasts are ~ 200 nautical miles, and the averaged intensity (maximum wind speed) errors are ~ 15 – 20 knots. To evaluate the state-of-the-science hydro- and morphodynamic models, reanalysis-quality data sets of tropical cyclone track, intensity, and wind fields are needed that have very small errors in the meteorological forcing. As an example, a methodology has been developed to produce very accurate tropical cyclone fields (intensity, track, and wind fields) using the US Navy's Coupled Ocean–Atmosphere Mesoscale

Prediction System for Tropical Cyclones (COAMPS-TC) (Doyle et al. 2012, 2014), which has been utilized by hydro- and morphodynamic models (e.g., Hegermiller et al. 2019).

3.3. Water Levels and Currents

Nearshore and coastal conditions are affected by water levels and currents driven by large-scale processes, including tides, winds, barometric pressure, and thermohaline circulation. Most of these processes are well understood and can be adequately modeled, but some details can become important during extreme events, as changes in water levels may cause a change in the Sallenger regime. Water elevation due to the inverse barometer effect can become the dominant component of storm surge on steep coasts with no shelves (Ponte 1992). Olabarrieta et al. (2017) and Shi et al. (2020) have shown that significant (~ 1 m) variations in total water levels with timescales of minutes and spatial scales of hundreds of meters can be generated by meteotsunamis triggered by spiral rainbands associated with tropical cyclones. The resulting small-amplitude (a few centimeters), very-low-frequency water-level fluctuations that can modulate infragravity waves and runup were observed on the Texas coast during Hurricane Harvey (2017) by Anarde et al. (2020). Forerunner (Ekman) surge forced by alongshore winds and the Coriolis effect can elevate water levels well before storms arrive (e.g., Kennedy et al. 2011), causing back-barrier lagoons to flood more easily, which leads to outwash (Goff et al. 2010, Sherman et al. 2013, Harter & Figlus 2017, Over et al. 2021). Other contributors to unusual water levels include baroclinic gradients (Pringle et al. 2019) and barotropic waves generated by moving fronts (e.g., Mercer et al. 2002).

Large-scale ocean currents, such as the Gulf Stream, Kuroshio, and Agulhas currents, influence wave propagation (e.g., Holthuijsen & Tolman 1991, Wandres et al. 2017, Rapizo et al. 2018) and, in the case of the Gulf Stream, have been linked to short-term but significant anomalies in coastal water levels (e.g., Ezer et al. 2017). Along the US East Coast, the Gulf Stream modulated coastal water levels by nearly 20 cm and modified incident-wave directions by 15° during Hurricane Matthew (2016) (Hegermiller et al. 2019). Furthermore, mesoscale circulation features, which are often unresolved in ocean-scale models, have been increasingly identified as important for modifying wave dynamics (e.g., Arduin et al. 2017, Romero et al. 2020). It is important to accurately model the timing of storm-induced water-level anomalies relative to astronomical tidal phase, as the arrival of surge at high tide may result in morphological changes associated with the overwash or inundation regimes, whereas the arrival of surge at low tide may result in changes within the swash or collision regimes.

Many of the processes affecting coastal water levels are well understood and can be accurately modeled if the forcing and boundary conditions are well constrained. The leading causes of poor model skill here are inaccurate bathymetry (especially dune-crest elevations, which determine, in part, the Sallenger regime) and insufficient model resolution. In the coastal ocean, bed friction can also exert strong control on hydrodynamics, though it is often unknown and used as a tuning parameter in hydrodynamic models (Fringer et al. 2019). As model resolution has increased with nesting and computational power, understanding of the importance of smaller-scale ocean features in coastal processes has expanded (Ganju et al. 2011). At the regional and local scales, additional factors may influence nearshore and coastal water levels and currents, such as the discharges from river mouths, estuaries, or tidal inlets.

Extreme wind speeds, such as those during hurricanes, push the limits of surface wind stress formulations (Bryant & Akbar 2016, Curcic & Haus 2020), affecting the accuracy of modeled surge and wave fields (e.g., Moon et al. 2009, Olabarrieta et al. 2012). In particular, it has proved difficult to close the energy budget at the atmosphere–ocean boundary due to the inability to measure each component in the field and the challenges associated with deploying instrumentation under

extreme conditions. Surface stresses are dependent on the ocean surface drag coefficient, which is poorly understood for extreme conditions and has been parameterized to vary with the wind speed, wave conditions, and even rainfall (Bryant & Akbar 2016 and references therein).

3.4. Waves and Wave-Driven Flows

Waves are ubiquitous in the coastal zone and—together with wind- and tide-driven currents—provide much of the energy that ultimately drives morphodynamic change across all of the Sallenger regimes. This section describes aspects of waves that are key to morphodynamic modeling.

3.4.1. Incident waves (seas and swell). Winds over the ocean exert a stress on the sea surface that generates short-period waves (seas), which, through nonlinear interactions, develop into longer-period waves (swell). Together, these waves form a spectrum in the incident band (2–25 s; Holthuijsen 2007). As waves propagate over the deep ocean, they can break due to steepening (whitecapping), redistribute energy over wave frequencies through wave–wave interactions, and interact with currents. As seas and swell approach shallower water, they increase in height (shoal), become more asymmetric (with higher peaks than troughs), change direction (refract) toward the shoreline, and ultimately break due to depth limitations. As they shoal and break, waves impart momentum to the water column that drives currents, generates wave-induced turbulence, and exerts shear stress on the bottom that can resuspend sediment, generate gradients in sediment transport, and ultimately cause morphodynamic change (Roelvink & Reniers 2012, Davidson-Arnott et al. 2019).

Numerical modeling of coastal hydrodynamics requires the ability to simulate dominant wave processes over a range of spatial scales and across hydrodynamic regimes and to parameterize other processes that are less important, not well understood (such as depth-limited breaking), or computationally too expensive to model (such as triad and quadruplet wave–wave interactions). As the dominant physics change from deep water to intermediate and shallow water, including the surf zone, coupling different models or different model modes becomes necessary to accurately simulate the waves that drive coastal morphological change. Because wave-driven processes contribute significantly to the total water level (e.g., Stockdon et al. 2006), they determine in large part the Sallenger regime and the timing of changes between regimes.

On the ocean scale, uncertainty in hydrodynamic forcing stems from parameterization of the source, sink, and redistribution formulations for wave energy over the spectrum. Source, sink, and redistribution terms for wave energy are sufficient to resolve bulk wave characteristics with predictive skill but poorly capture wave spectral characteristics. There have not been recent major advances in the development of these formulations (see Cavaleri et al. 2018, 2020, and references therein). However, due to increased computational power, there have been large advances in the size and resolution of the areas that can be modeled and the processes that can be simulated directly (figure 2.4.1 in Cavaleri et al. 2018).

3.4.2. Shoaling-wave transformations. Shoaling transforms waves into nonlinear shapes that generate skewed and asymmetric orbital velocities that can drive sediment transport. Wave shape is not resolved in wave-averaged models, such as SWAN and WAVEWATCH III, so methods have been devised to estimate skewness and asymmetry from local wave properties (Rienecker & Fenton 1981, Isobe & Horikawa 1982, Doering & Bowen 1995, Doering et al. 2000, Ruessink et al. 2012). Doering & Bowen (1995) first parameterized wave skewness and asymmetry using the local Ursell number U_r , and Ruessink et al. (2012) extended that parameterization using a large data set from barred beaches with significant wave heights ranging from 0.05 to 3.99 m

($0.04 < U_r < 24.8$). However, there is a lot of scatter in the observations, which Rocha et al. (2017) attributed to wave-propagation history. Using wave-flume measurements and numerical simulations from the SERR1D model (Cienfuegos et al. 2006, 2007), Rocha et al. (2017) found a correlation between the wave nonlinearity parameters and the offshore wave steepness, beach slope, and spectral bandwidth, confirming earlier studies by Elgar & Guza (1985) and Norheim et al. (1998). The parameterization of Rocha et al. (2017) extends that of Ruessink et al. (2012) by incorporating nonlocal wave parameters and beach slope.

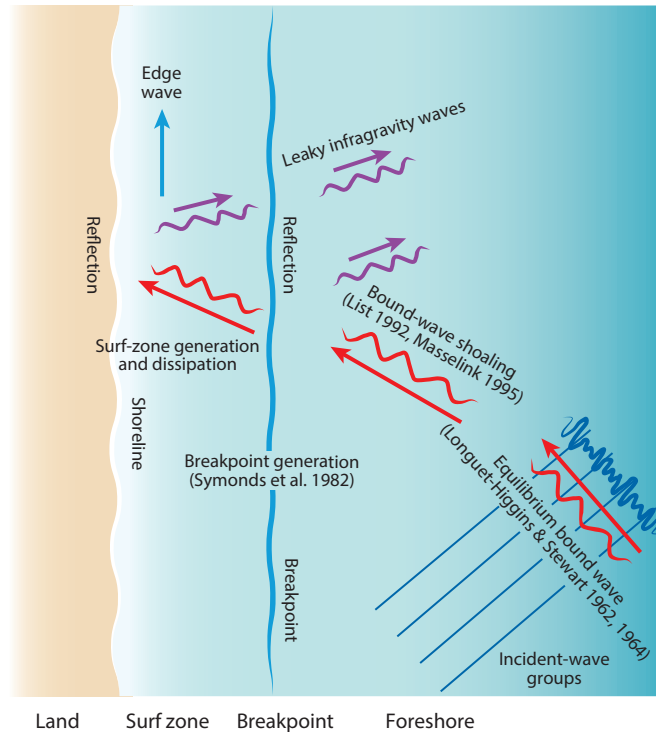
3.4.3. Infragravity waves. Incident waves with varying frequencies and directions can form wave groups—sequences of waves with higher and then lower amplitudes (**Figure 3**). As these waves exert a stress on the water column (the radiation stress; Longuet-Higgins & Stewart 1962), the mean surface is depressed under the high waves and elevated under the low waves. This undulation constitutes a wave with a period of ~ 25 – 250 s that travels with the wave groups and is called a bound infragravity wave (Munk 1949, Tucker 1950) (see the sidebar titled Infragravity Wave Motions). Bound infragravity waves gain energy through the shoaling mechanism as wave groups move into shallower water (List 1992, Masselink 1995, Janssen et al. 2003, Battjes et al. 2004). Ultimately, they are released from the group as the incident waves dissipate and form free infragravity waves that may reflect from the shore to propagate seaward. Energy at infragravity-wave frequencies can also be generated in the nearshore by modulations in wave breaking at the wave-group scale, known as the breakpoint mechanism (Symonds et al. 1982). In the surf zone itself, infragravity waves gain energy by radiation stress forcing (Foda & Mei 1981, Schäffer & Svendsen 1988) but may also lose energy through bottom-friction dissipation (Henderson & Bowen 2002) and infragravity-wave breaking (van Dongeren et al. 2007).

As a result of these processes, infragravity waves can have considerable wave heights (~ 1 m) during storm conditions (see references summarized in Billson et al. 2019); modulate water levels, short-wave characteristics (e.g., Tissier et al. 2015), and surf-zone velocities; and exert fundamental control on wave runup (e.g., van Gent 2001, Stockdon et al. 2006). Whereas Bertin et al. (2019, figure 11) suggest that infragravity waves do not contribute significantly to morphological change in Sallenger's swash and inundation regimes, their potential relevance for beach cusps and sandbar formation has been studied since the 1980s, and they have been linked to bar migration (e.g., Roelvink & Stive 1989). They are clearly important in the collision and overwash regimes, where they contribute to dune erosion (e.g., van Thiel de Vries et al. 2008, Roelvink et al. 2009), inlet closure (Bertin et al. 2019), and the formation of washover deposits (Baumann et al. 2017). (For recent reviews of infragravity-wave dynamics and their influence on morphology, see Bertin et al. 2018, Billson et al. 2019, and references therein.)

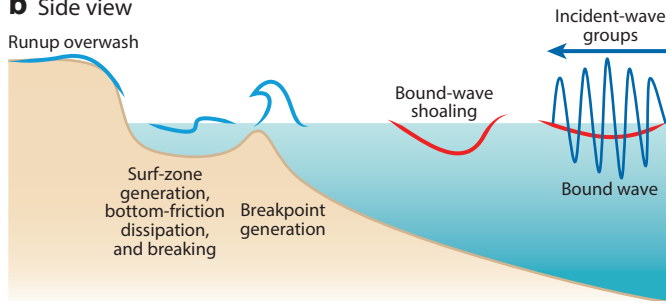
The inclusion of infragravity waves in models such as XBeach (Roelvink et al. 2009) and the In-Wave component of COAWST (M. Olabarrieta, C.A. Hegermiller & J.C. Warner, manuscript in review) may be the most important advance in coastal morphodynamic models in the last 15 years. In these models, wave groups are statistically generated from short-wave spectra, assuming random phases. The resulting infragravity wave is solved via an analytical solution (Herbers et al. 1994, van Dongeren et al. 2003) and imposed as water-level variations on the offshore boundary of the model domain. Infragravity-wave energy generated by breakpoint forcing is resolved in the models either by radiation stress or vortex force formulations. The inclusion of infragravity waves and associated sediment transport in nearshore models requires high spatial resolution and short time steps, which presently constrains the spatial and temporal scope of model simulations.

3.4.4. Wave-driven flows. Wave-generated flows are uniquely important in coastal models. As waves shoal and break, kinetic energy is dissipated into foam, turbulence, and heat and converted

a Top view



b Side view



Surf-zone generation (Foda & Mei 1981)
 Bottom-friction dissipation (Henderson & Bowen 2002)
 Infragravity-wave breaking (van Dongeren et al. 2007)

Figure 3

Schematic of infragravity waves, illustrating their formation from incident waves and breakpoint generation, followed by shoaling, refraction, reflection, breaking, and dissipation.

into the forward and rotational momentum of rollers, which are turbulent water masses that slide down the faces of broken waves and contribute to the energy and momentum budgets of the surf zone. The net effect of breaking waves on average momentum is called the radiation stress (Longuet-Higgins & Stewart 1964). The alongshore component of radiation stress drives alongshore flows. The cross-shore component is balanced on a closed coast by a pressure

gradient, producing an increase of the mean water level toward the shoreline, called the wave-induced setup. Radiation stress is formulated for depth-average flows. Alternate approaches are required to resolve the forcing for 3D flow and include the formulations based on the generalized Lagrangian mean and vortex force (Lane et al. 2007). The generalized Lagrangian mean was introduced by Andrews & McIntyre (1978), with the approach of averaging over disturbance positions of the fluid particle, which is valid over the complete water column. Ardhuin et al. (2008) developed a practical set of equations based on the work of Dingemans (1997), which have been applied in several studies. A recent variation of the generalized Lagrangian mean approach has been implemented in Delft3D (Nguyen et al. 2021). The vortex force approach was developed by Craik & Leibovich (1976) and splits the wave-averaged effects into gradients of a Bernoulli head pressure adjustment to accommodate incompressibility (Lane et al. 2007) and a vortex force, which, after wave averaging, is a function of wave-induced Stokes drift and flow vorticity. This approach allows for these conservative terms to be split from other, nonconservative wave-dissipation-induced acceleration contributions and has been implemented in COAWST (Kumar et al. 2012, following McWilliams et al. 2004 and Uchiyama et al. 2010).

The volume of water in the rollers is carried toward the shore and returned in rip currents or below the troughs of the waves as an undertow current. The generation of rollers is modeled as a function of a percentage of wave breaking and roller dissipation following one of several semiempirical formulations (Walstra et al. 1996, Roelvink et al. 2009). Considerable effort has gone into modeling the vertical distribution of the cross-shore and longshore wave-driven current, with key ingredients being the near-surface stress associated with rollers, the vertical distribution of turbulence and near-bed streaming, and bottom friction (e.g., Kumar et al. 2012). Given along-shore variations in bathymetry or wave forcing, the return flow may concentrate into rip currents (MacMahan et al. 2006). Gradients in the alongshore component of the radiation stress drive a nearshore longshore current that can be $O(1 \text{ m/s})$ in magnitude.

3.5. Sediment Transport

Sediment transport in nearshore environments is driven mainly by short waves (seas and swell), infragravity motions, and wave-induced currents. The short timescales of seas and swell are a computational challenge for models that must integrate their effects over storm-event timescales, so most morphodynamic models consider time-averaged waves and resolve more slowly varying currents. From a sediment-transport perspective, infragravity waves act on a timescale that blurs

INFRAGRAVITY WAVE MOTIONS

Infragravity waves, also known as surf beat, are long-period waves (periods of $\sim 25\text{--}250 \text{ s}$) generated by the interaction of short waves to form wave groups. Since their discovery in the late 1940s, they have been thought to cause a range of phenomena, some of which are now attributed to other processes. But what has remained a well-established mechanism is the role of infragravity runup in elevating water levels at the coast, particularly during storms. In addition, the elevated water surfaces generate the undertow responsible for offshore transport, and the modulation of short waves drives cross-shore transport in both directions. Most importantly, the increased water levels can push storm conditions into a higher Sallenger regime, elevating swash conditions to collision or collision to overwash. The incorporation of infragravity motions into coastal sediment-transport models like XBeach and COAWST may be the most significant advance in coastal model physics in the last two decades and has led to substantial improvements in our ability to model extreme events (e.g., figure 11 in Bertin et al. 2018).

the distinction between wave motions and mean currents, which is one reason that resolving them has improved model skill.

Sediment-transport formulations can represent the total load or split it among bedload and suspended-load models. Both modes of transport are important for morphological evolution (e.g., Reniers et al. 2013). Bedload transport occurs with high sediment concentrations very close to the seabed, so bedload flux is parameterized by local near-bed flows in the form of mean currents, wave-orbital motions, and boundary-layer streaming acting on sediment properties. By contrast, suspended-sediment transport, which is dominant during storm events, is the product of current velocities and relatively small sediment concentrations over the entire water column. Models of suspended-load flux explicitly account for the spatial variabilities of waves, turbulence, currents, and bathymetry by solving the advection–diffusion–settling equation for the conservation of sediment mass, either in a depth-averaged formulation (Galappatti & Vreugdenhil 1985) for 2D models such as XBeach (Roelvink et al. 2009) or in a depth-resolving formulation in 3D models such as COAWST (Warner et al. 2008b). Suspended-sediment formulations include a mechanism for depositional fluxes to the seafloor (based on the product of near-bed concentration and settling velocity) and resuspension from the seafloor, represented by an erosional flux or via changes in a near-bed reference concentration. Both approaches usually rely on the wave-stirring concept (e.g., Soulsby 1997; van Rijn 2007a,b), which is driven by bottom shear stress generated by the combined influence of waves and currents (Smith 1977, Grant & Madsen 1979). In shallow water, turbulence produced by breaking waves that penetrates to the seabed can further enhance resuspension (Roelvink & Stive 1989).

Bedload transport under shoaling waves is influenced by a wave skewness that generates asymmetry in velocity and acceleration over the wave cycle (Nielsen 1992) (**Figure 4**), horizontal pressure gradients (Drake & Calantoni 2001, Hsu & Hanes 2004, Foster et al. 2006), and bedload streaming (Longuet-Higgins 2005; Nielsen 2006; Kranenburg et al. 2012, 2013; Fuhrman et al. 2013). The classic quasi-steady energetics approach to wave-induced bedload transport of Bailard & Inman (1981) captures only velocity asymmetry. Kim et al. (2018, 2019) showed that progressive wave streaming contributes an additional 60–300% of the total load onshore transport rate, depending on wave-orbital velocity skewness and asymmetry. Wave models that simulate wave-averaged action density, such as SWAN and WAVEWATCH III, cannot represent the shoaling transformations that generate skewness and asymmetry, but parameterizations of wave asymmetry based on local conditions (water depth and wave height and period; van Thiel de Vries et al. 2008, Ruessink et al. 2012) have been used to determine wave-orbital velocities over all portions of the wave period (**Figure 4**). These velocities can then be used in bedload transport formulae like the SANTOSS equation (Ribberink et al. 2010, van der A et al. 2013). Despite the detailed physics represented in these equations, modelers have found it necessary to modify the results with leading coefficients: In XBeach, the facua calibration coefficient adjusts the effect of wave shape on cross-shore transport, and in COAWST, separate coefficients modify the wave- and current-induced transport rates. Some studies have found that the same value of the XBeach facua parameter performed well in simulations at different sites (van der Lugt et al. 2019), but others have found that different values were needed to successfully model onshore versus offshore transport rates depending on the energy of the incoming waves (Rafati et al. 2021). The need for model-tuning parameters that vary with wave conditions indicates that not all the physics are being captured in these parameterizations and reinforces the argument that nonlocal conditions, wave-propagation history, and sediment response are important factors in determining wave-shape-induced transport.

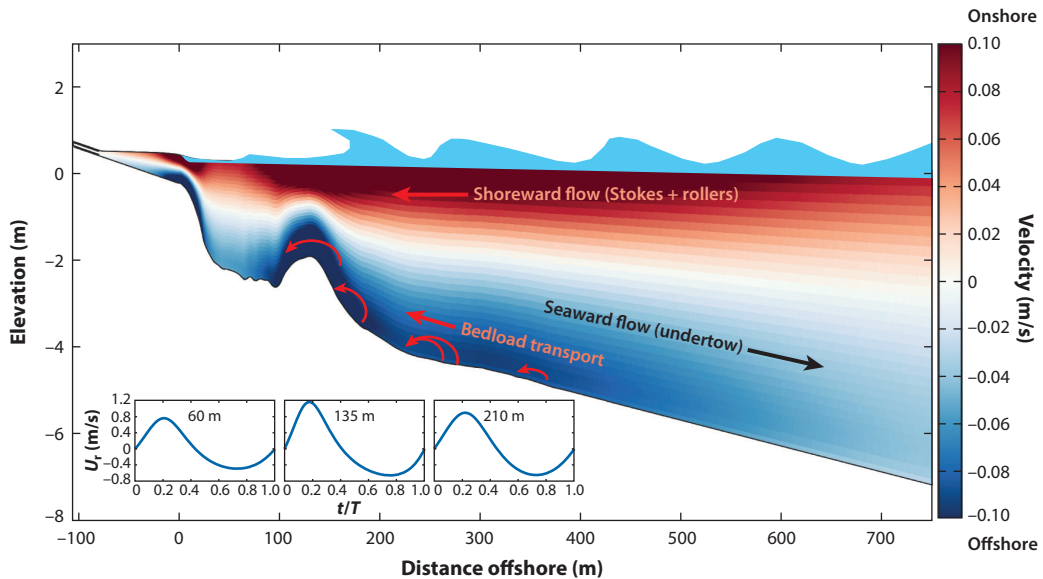


Figure 4

Schematic of wave shoaling and vertical circulation in the nearshore, showing the bed profile along a cross-shore transect measured in the DUCK94 experiment on October 12, 1994, and the simulated flow field (Kalra et al. 2019). Cross-shore velocities are shown with shading and arrows. The inset graphs illustrate intrawave near-bed velocities over wave period T at three cross-shore locations, calculated from the Ursell number U_r of waves in the SWAN model according to Abreu et al. (2010) and Ruessink et al. (2012). **Supplemental Video 1** shows the development of the nearshore circulation and evolution of the nearshore and beach bathymetry and topography at Matanzas, Florida, during Hurricane Matthew.

Supplemental Material >

3.6. Vegetation and Hydraulic Roughness

Coastal vegetation (submerged aquatic vegetation, marsh vegetation, dune grasses, and woody vegetation) influences morphological evolution during storms in multiple ways: Vegetation impedes flow, damps wave motions, reduces sediment resuspension, affects near-bed turbulence, and stabilizes the seabed (Hemminga & Duarte 2000, Wamsley et al. 2010, Carr et al. 2012). On longer timescales, vegetation reduces coastline erosion and aids dune growth. Two general approaches have been proposed to account for the effect of vegetation on fluid dynamics and thus morphological change: (a) parameterize the effect of vegetation as enhanced hydraulic roughness, and (b) resolve the effects of vegetation using explicit formulae to model hydrodynamics in the vegetation canopy.

The first approach aims to translate land-cover information on vegetation type, usually derived from remote sensing, to hydraulic roughness (de Vet et al. 2015, Schambach et al. 2018). Roughness values are typically parameterized by a bed-friction coefficient (e.g., Manning's n or the Chezy coefficient). Conversion from land cover to roughness is done through conversion tables (e.g., Arcemet & Schneider 1989, Mattocks & Forbes 2008). This allows the initial bed friction to vary spatially and, in some models, change as land cover evolves with the erosion or burial (van der Lugt et al. 2019). Semisupervised machine learning techniques such as the conditional random field method (Buscombe & Ritchie 2018) can help map land cover from imagery, but the initialization and evolution of roughness values remain subjective. The overall impact of the bottom roughness on the simulated hydrodynamics (and therefore morphodynamics) varies depending on the source of the land-cover data, the method for converting it to roughness, and the

geographic distribution of roughness in the affected area (Ferreira et al. 2014, Machineni et al. 2019). **Supplemental Video 2** shows an example of the effect of varying the bottom-roughness parameterization in a coupled hydro- and morphodynamic model simulation of the passage of Hurricane Ike over Bolivar Peninsula in Galveston, Texas (from the simulation described in **Figure 7** below; see Section 5.2.4).

The second approach aims to explicitly resolve stem shape and density and use these in momentum equations to model drag and turbulence (e.g., van Rooijen et al. 2016, Beudin et al. 2017). Vegetation affects wave-induced streaming (Luhar et al. 2010, Luhar & Nepf 2011) and the vertically varying production and dissipation of turbulence (Uittenbogaard 2003). The effect of vegetation on wave damping was derived parametrically by Dalrymple et al. (1984) and Mendez & Losada (2004) and has been implemented in spectral wave models such as SWAN (Suzuki et al. 2012). Vegetation effects on infragravity waves are implicitly accounted for by bottom drag, which is considered appropriate because the wave-orbital excursion of infragravity waves is generally much larger than the spacing between vegetation (Svendsen 2006). Although most of these explicit approaches have been developed for submerged aquatic vegetation (see Nepf 2012), modelers (e.g., C.A. Hegermiller, J.C. Warner, M. Olabarrieta, C.R. Sherwood & T.S. Kalra, manuscript in review, using the model described in Beudin et al. 2017) are adjusting the physical parameters to adapt them to emergent vegetation such as dune grasses and mangroves. Both the empirical and physics-based approaches have been shown to improve model skill, as discussed below.

3.7. Wetting and Drying

A robust wetting and drying procedure is required for simulating the uprush and backwash during swash and collision regimes, the overtopping during the overwash regime, and the inundation of marshes and tidal flats by tides and surge. The procedure must be able to handle both subcritical and supercritical flows without numerical oscillations. In XBeach, this has been achieved by adopting explicit upwind schemes with automatic time steps (similar to Stelling & Duinmeijer 2003), which is especially suitable for drying and flooding and which allows a combination of sub- and supercritical flows. This scheme guarantees positive water depths if the Courant–Friedrichs–Lewy criterion is observed and removes the need for special flooding procedures. The original implementation applied first-order discretizations and momentum conservation; later implementations include second-order advective terms and a switch (as in Stelling & Duinmeijer 2003) between momentum conservation and conservation of energy head. Validation of the implemented scheme was provided for runup cases by Roelvink et al. (2009) and for a range of inundation and dam-break problems by Hartanto et al. (2011). A slightly different approach is required for COAWST because of its staggered grid, but an effective numerical scheme has been implemented and tested by Warner et al. (2013).

3.8. Morphological Change

In this section, we describe how sediment transport is coupled with morphodynamic change and discuss techniques to speed up computational time.

3.8.1. The Exner equation. Morphological change is governed by the Exner equation (Exner 1920, 1925), a simplified version of the generalized sediment mass-balance equation (Paola & Voller 2005), which states that porosity-corrected bed elevation changes are caused by horizontal divergence in sediment flux. The main challenge in solving the Exner equation is modeling sediment flux, which includes both bedload and suspended-sediment transport (Paola & Voller 2005, Mendoza et al. 2017), based on at least partly empirical formulae (Kaveh et al. 2019) that

require calibration (Mendoza et al. 2017, Baar et al. 2019). Even with accurate transport formulae, attention to the numerical discretization used to solve the Exner equation is required; poorly formulated methods can lead to excess dispersion and bed elevation oscillations (Johnson & Zyserman 2002, Callaghan et al. 2006, Chiang et al. 2011).

3.8.2. Morphological acceleration. Numerical simulations of long-term morphological change can be computationally demanding if done by brute force (e.g., Safak et al. 2017), so methods have been developed to speed up morphodynamical models (Lesser et al. 2004, Roelvink 2006, Ranasinghe et al. 2011, Roelvink & Reniers 2012, Luijendijk et al. 2019, Morgan et al. 2020) using a combination of two approaches: input reduction (or input schematization; e.g., Walstra et al. 2013, Luijendijk et al. 2019) and morphological acceleration (Lesser et al. 2004, Roelvink 2006, Ranasinghe et al. 2011). Input reduction seeks to force the model using representative conditions (e.g., the average wave height) or only the conditions that effect morphodynamic change (e.g., waves greater than some threshold). The morphological acceleration factor assumes a linear relationship between the divergence in horizontal sediment flux and the change in bed elevation over some effective time and multiplies the bed changes by a morphological acceleration factor (M_f) to simulate change over a longer time period. For example, simulations made over a tidal cycle with representative tidal conditions (from input reduction) with an M_f of 4 are intended to represent morphological change for two days. The key assumption is that bed changes, even after being multiplied by M_f , do not significantly change the sediment-transport rate—or, more specifically, the divergence in sediment transport. One method used in storm simulations is to divide the time series of wave spectra into hours and, for each hour, to simulate waves for only $1/M_f$ hours. The time axis of the other forcing conditions (water level, wind speed and direction, etc.) is shrunk by the same M_f . Experience in many actual cases has shown that an M_f of 5–10 yields very small deviations relative to brute-force simulations. Although M_f values of up to 100 have been used successfully in long-term simulations (e.g., Lesser et al. 2004, van der Wegen & Roelvink 2008), extreme events have strongly time-varying forcing conditions that preclude the use of a high M_f , and the events are often short enough that simulating the entire forcing time series is computationally affordable.

4. MODEL SKILL AND UNCERTAINTY

The greatest challenge in assessing the skill of morphological models is often the lack of accurate and timely data for comparison. But even when good data are available, assessing morphological model skill and uncertainty is tricky. Whereas hydrodynamic model output can be compared objectively to observed integral parameters (wave heights, wave periods, etc.) or time series, it is difficult to assess morphological model skill because the output concerns changes in shape (Sutherland et al. 2004). Point-by-point metrics based on the mean-squared difference between modeled and observed elevation maps, such as the Brier skill score (van Rijn et al. 2003, Stow et al. 2009), tend to favor model results that underestimate the variance of changes (Bosboom et al. 2014). One approach from meteorology is to assess the magnitude of displacement required to minimize the difference between the model and observations, which can produce multiple metrics over a range of spatial scales (Bosboom & Reniers 2014). For the case of storm-driven morphodynamic elevation change, volume changes and the locations and elevations of dune features can be considered. Categorical approaches can help with broad-scale comparison between models and observations (C.A. Hegermiller, J.C. Warner, M. Olabarrieta, C.R. Sherwood & T.S. Kalra, manuscript in review) (**Figure 5**). Unfortunately, because different metrics are often selected, it is difficult to compare skill across model applications.

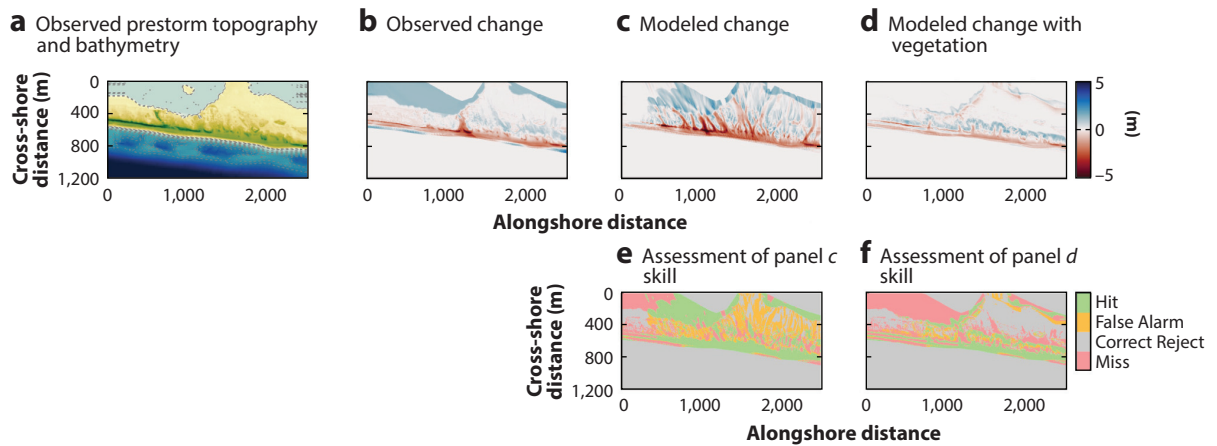


Figure 5

(a) Observed topography and bathymetry of the Wilderness Breach on Fire Island, New York, before Hurricane Sandy (2012). (b) Observed change due to Hurricane Sandy, where red indicates erosion and blue indicates deposition. Note that the apparent back-barrier deposition is likely an artifact. (c) Modeled change from COAWST simulations that did not account for effects of land-cover variation. (d) Modeled change from COAWST simulations with the vegetation module activated. (e) Assessment of the skill of the modeling shown in panel c, where Hit indicates that the model correctly predicted observed erosion or deposition, False Alarm indicates that the model predicted erosion or deposition that was not observed, Correct Reject indicates that the model correctly predicted no change, and Miss indicates that the model did not predict observed erosion or deposition. Note that accounting for vegetation effects on hydrodynamics and sediment transport minimizes the False Alarm areas associated with overwash. (f) Assessment of the skill of the modeling shown in panel d.

Accurate pre- and poststorm measurements are required to initialize models and assess changes. Nearshore bathymetry is measured by various methods (lidar, occupied and autonomous floating vessels with sonar, bottom-crawling vehicles, and inference from wave motions). All of these have trade-offs in terms of expense, areal coverage, resolution, accuracy, and timeliness, and none are currently able to provide bathymetric updates at the peak of extreme storms. Poststorm observations must be made immediately (within days) after the event, before natural or human processes of recovery can change the landscape (Lazarus & Goldstein 2019). The recent increase in rapid-response flights like the NOAA National Geodetic Survey emergency-response flights (<https://storms.ngs.noaa.gov>) and the ability to process those images using modern multiview photogrammetry (also known as structure from motion) can provide timely information about subaerial conditions, but sometimes that is not fast enough, as repair efforts can start the day after an event (Sherwood et al. 2018). New breaches tend to evolve rapidly: The Wilderness Breach on Fire Island changed remarkably in the days, weeks, and months after Hurricane Sandy (Hapke et al. 2017), and the data available for model validation (summarized in van Ormondt et al. 2020) were collected at various points during the inlet evolution. Determination of the extent of storm-induced scour in channels is difficult because scour can continue after the storm passes, and channel depths cannot be monitored with subaerial techniques. Model parameterizations governing scouring are therefore calibrated on specifically designed controlled experiments, such as those described by Visser (1994) for a flow-dominated breach and Schweiger et al. (2020) for a wave-dominated breach through a dune.

Uncertainty in initial conditions, forcing, or model formulations combine to compound model errors. We often lack spatially resolved hydrodynamic observations in the study area: Wave buoys and water-level measurements are sparse, and there are often few current measurements

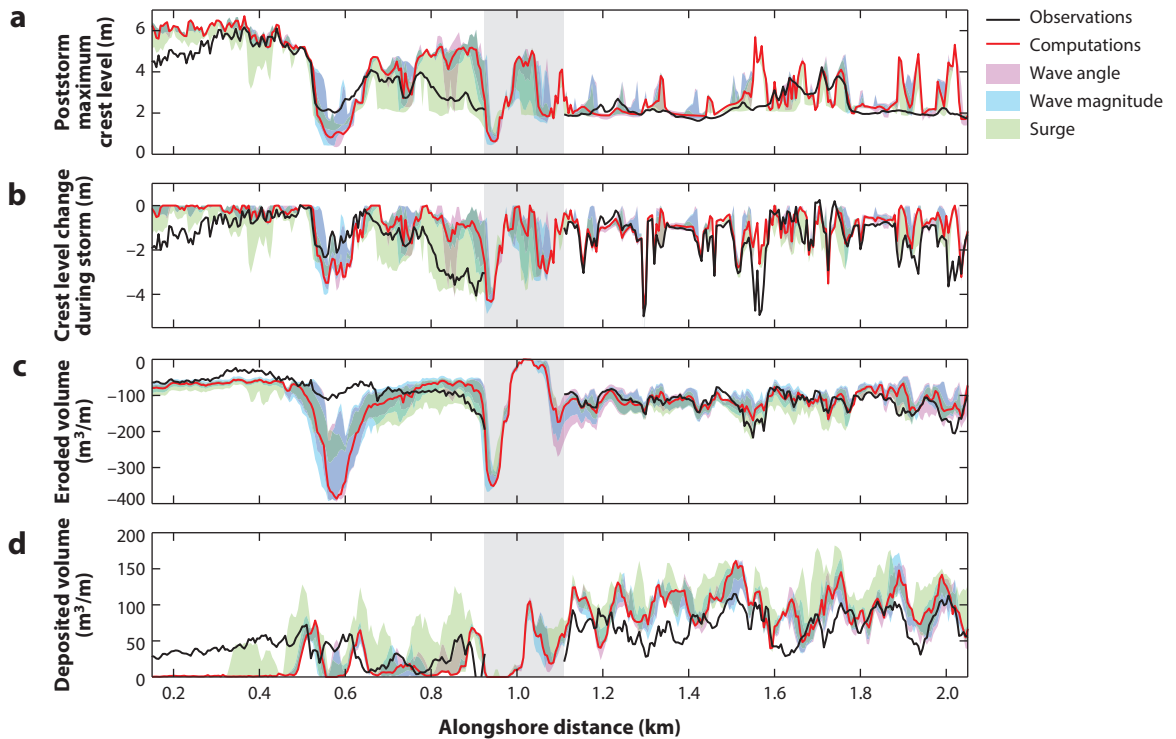


Figure 6

Sensitivity of XBeach-computed dune shape change to uncertainty in offshore forcing during Hurricane Sandy (2012) at the Wilderness Breach on Fire Island, New York: (a) poststorm maximum crest level (meters above NAVD 88), (b) crest level change throughout the storm, (c) total eroded volume in the dune section, and (d) total deposited volume in the dune section. Observations are shown in black, and base computations are shown in red. The shaded areas indicate the variability of the parameters as a result of variations in hydrodynamic forcing: Wave angle (purple) shows a variation of $\pm 5^\circ$ in the offshore mean wave direction, wave magnitude (blue) shows a $\pm 10\%$ variation around the predicted offshore significant wave height, and surge (green) shows a $\pm 10\%$ variation of predicted offshore water levels. The observed breaching extent is indicated in gray shading because no subaerial poststorm observations are available there. **Supplemental Video 3** shows the simulated hydro- and morphodynamics at the Wilderness Breach during the event for best-estimate parameter settings. Figure adapted with permission from van der Lugt et al. (2019); copyright 2019 Elsevier.

to constrain the model outcome. Uncertainty in initial and forcing conditions propagates into model results; for example, a study by van der Lugt et al. (2019) demonstrated the limitations of single deterministic model runs in forecasting storm impact (**Figure 6**).

Supplemental Material >

5. OUTLOOK AND TRENDS

5.1. Processes

Morphodynamic models have become both wider and deeper—wider as more processes are added (like the effects of vegetation or even bulldozers; Lazarus & Goldstein 2019), and deeper as detailed physics replace earlier parameterizations (e.g., vortex forcing and incident-wave runup) and more information on initial and boundary conditions becomes available. We cite this as one of the overall trends in coastal models in Section 5.2. In this section, we discuss some additions and improvements.

5.1.1. Wave-resolving models. One solution to the difficulty in parameterizing wave behavior in shallow water is to resort to wave-resolving models such as MITgcm, TRIM, SUNTANS, SWASH, CROCO, NHWAVE, FUNWAVE, Celeris, and XBeach-NH+ (Marshall et al. 1997, Casulli 1999, Fringer et al. 2006, Zijlema et al. 2011, Debreu et al. 2012, Ma et al. 2014, Malej et al. 2015, Tavakkol & Lynett 2017, and de Ridder et al. 2021, respectively), which are capable of skillfully simulating the shapes and orbital motions of nonlinear waves (e.g., Tissier et al. 2011, Smit et al. 2014) and, critically, can resolve water-level variations associated with setup and swash. Although most wave-resolving models lack sediment-transport formulations and are still too computationally expensive to simulate regional-scale nearshore morphodynamics, we anticipate that this will change, and that wave-resolving models will be improved to incorporate breaking-induced turbulence, be coupled with sediment-transport formulae (e.g., van der A et al. 2013, Fringer et al. 2019), and become more common components of coastal morphodynamic models.

5.1.2. Soil mechanics, groundwater, and dune vegetation. The mechanics of dune and foreshore erosion are represented by relatively simple parameterizations based on, for example, wave impact (Overton & Fisher 1988), dry cell erosion, or critical slope (Roelvink et al. 2009). Although the primary controls on dune scarping (relative water level, beach width, dune volume, and beach slope; Palmsten & Holman 2011, Héquette et al. 2019, Davidson et al. 2020) are incorporated in storm-event models (e.g., Cohn et al. 2019b), secondary factors (Davidson et al. 2020), such as vegetation, root mass, the presence of wrack or woody debris, and compaction, are often not. Although simple parameterizations have provided adequate results in terms of slumping rate and postevent profile shape, more physically based modeling of dune and foreshore processes based on soil-mechanics principles may be the key to improving models of dune stability and beach trafficability. Recent progress in sensors to rapidly characterize key soil properties, such as sediment strength and its relationship to wave energy, friction angle, and moisture content (Stark et al. 2017, Albatal et al. 2019), may lead to improved modeling of soil mechanics in morphodynamic models. However, with improved physical description of these processes will come a demand for more data regarding soil moisture, geological framework, and sediment characteristics, for which observations at the appropriate scale are often lacking.

5.1.3. Hydrologic coupling. Significant rainfall on land and over water often accompanies storms, with quantifiable contributions to water levels in back-barrier lagoons or sounds by direct precipitation (Rey et al. 2020), elevated groundwater tables, and potential for compound flooding from runoff in large watersheds. Surface runoff and elevated groundwater can impact beach stability and lead to barrier-island flooding (Housego et al. 2018, Huizer et al. 2018). Coupling of hydrologic, groundwater, and ocean hydrodynamic models will provide improved boundary conditions and increase our ability to predict total water levels for inundation and morphological change models (Santiago-Collazo et al. 2019, Bakhtyar et al. 2020, Gori et al. 2020, Yin et al. 2020). Increased computational resources, improved nesting schemes, and use of input-reduced and reduced-physics approaches will support the inclusion of hydrological processes in coastal ocean modeling.

5.2. Trends

Here we summarize emergent trends in storm-impact models.

5.2.1. Community and open-source models. Early earth-science open-source models were developed in the 1990s to address air-quality modeling, climate prediction, and weather

forecasting (Voinov et al. 2010). Open-source ocean and nearshore models began to emerge in the late 1990s and early 2000s with ROMS, POM, and COHERENS, and the Community Sediment Transport Model project that would eventually become COAWST was launched in 2000 (Sherwood et al. 2000, 2002). Codes for models that were previously proprietary, such as Delft3D and TELEMAC, have been released, and since then, models have often been open source from their conception (e.g., XBeach and COAWST). The use and maintenance of models have become much easier with the advent of public source-code repositories like SourceForge and GitHub and the development of niche earth-science and marine model repositories, such as those hosted by the Community Surface Dynamics Modeling System (https://csdms.colorado.edu/wiki/Model_download_portal) and the OpenEarth initiative at Technische Universiteit Delft and Deltares (<https://www.deltares.nl/en/software/openearth>). Most of the models used for coastal morphodynamics research are open source, and we anticipate that this trend will continue.

5.2.2. Increased physical detail. The information presented above makes it clear that more processes are being included in models (see next section) and more physics are being included in the processes, replacing earlier parameterizations. Physics of infragravity waves, vortex forcing, wave shape, rollers, boundary-layer streaming, flows in submerged and emergent vegetation, land cover, and dynamic roughness have been incorporated in existing models, and we expect this trend of increasingly detailed physical processes to continue.

5.2.3. Inclusion of more and more-detailed processes. More processes are being incorporated into coastal morphodynamic models. In addition to those listed above, four models are capturing important features of aeolian dune formation and vegetation: the Coastal Dune Model (Durán & Moore 2013), AEOLIS (Hoonhout & de Vries 2016), Duna (Roelvink & Costas 2019), and Windsurf (Cohn et al. 2019a). Although aeolian transport plays a minor role relative to the wave-driven processes in storms, even during the recovery phase (e.g., Kombiadou et al. 2021), the inclusion of these processes will improve simulations on timescales of years to decades. The effects of wave growth due to local winds can also be included. Although additional wind-driven wave growth in the nearshore domain is negligible compared with transformation and dissipation processes, changes in the air–sea drag coefficient occur as waves shoal and break (Ginis et al. 2021). In lagoons behind reefs or in bays behind sandy barriers, the situation may be quite different, and both infragravity waves (not resolved by spectral wave models) and wind growth (not resolved in time-domain models) may be relevant (e.g., Drost et al. 2019). The role of structures in morphodynamic processes can also be included (e.g., Smallegan et al. 2016 for the case of a seawall in New Jersey). These and other processes (e.g., biological effects on sediment mobility and groundwater controls on dune and beach erosion) are being added to coastal morphodynamic models, making them more general.

5.2.4. Improved initial, lateral, and bottom-boundary conditions. The accuracy of coastal morphology models is highly dependent on the accuracy of the meteorological, wave, and hydrodynamic models by which they are forced, as well as the prescription of the initial and bottom boundary conditions. The hindcast and forecast skill of these models is increasing as the availability of computational power allows for higher resolution and less parameterization of physics in parent models, from which the lateral boundary conditions for the coastal morphology model are extracted. Additionally, parent models have expanded grid flexibility, allowing for stepwise refinement and making the nesting of high-resolution coastal morphology model

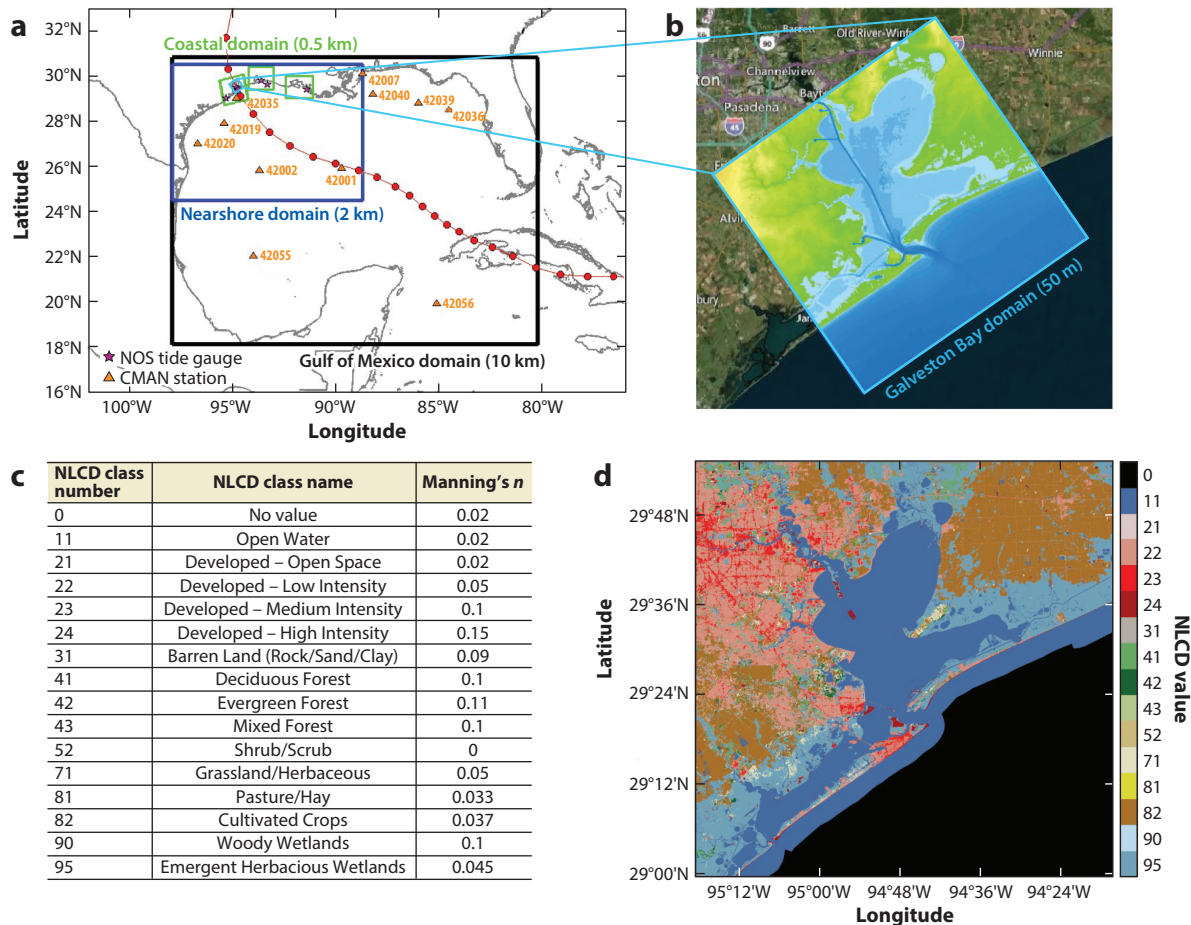


Figure 7

(a) Example of a nested domain simulation, where each of the three domains passes boundary conditions to its child domain. (b) The initial bathymetry of the innermost domain, as set by a high-resolution digital elevation model. (c) Manning's n bottom-friction coefficients assigned to NLCD values (Mattocks & Forbes 2008). (d) The NLCD values used to specify the initial bottom-roughness formulation in the model. Abbreviations: CMAN, Coastal Marine Automated Network; NLCD, National Land Cover Database; NOS, National Ocean Service. **Supplemental Video 2** shows an example of the effect of varying the bottom-roughness parameterization in a coupled hydro- and morphodynamic model simulation of the passage of Hurricane Ike over Bolivar Peninsula in Galveston, Texas.

domains more computationally feasible (**Figure 7**). The increasing availability of high-resolution bathymetry and land cover from remotely sensed sources allows for more accurate depths and hydraulic roughness in coastal regions. Databases can provide an estimate of the spatial variations in the bottom-friction coefficient due to land-cover type and sediment grain size, both of which play key roles in the fundamental processes of coastal morphology (**Figure 7**).

Grain size affects sediment mobility and bottom roughness, and therefore erosion and deposition patterns, and it also affects the slope of dune faces and beach profiles (Dean 1991). Many models can treat a range of sediment classes (e.g., Warner et al. 2008a). However, in extreme conditions, most noncohesive sediment particles will mobilize, so spatially resolved initial grain-size variations are not widely used because any variations in the mobilization patterns that would be due to grain-size differences are overshadowed by the hydrodynamics. Additionally, measurements

of grain size over entire model domains are rare, and therefore the initialization or validation of morphodynamic models with grain size is atypical (one exception is Reniers et al. 2013). Finally, differences in modeled morphology that might be associated with grain size may be obscured because the calibration of morphological models relies on sensitivity testing and reduction of error through adjustments of unconstrained parameters, including those related to grain size (e.g., bed roughness, bedload transport rates, settling velocities, and critical shear stresses), for which observations often are not available. We anticipate that more attention will be paid to the role of variable sediment characteristics as new mapping methods are developed and computational resources continue to become more available.

5.2.5. Data assimilation. Data assimilation is being increasingly incorporated into coastal morphology models. Direct inference of bathymetry from observations of the sea surface has been used since World War II (Williams 1947) and is now based on estimates of wave dissipation and/or wave celerity, current velocity, and shoreline location derived from video imagery (e.g., Stockdon & Holman 2000; Alexander & Holman 2004; van Dongeren et al. 2008; Wilson et al. 2010, 2014; Birrien et al. 2013; Holman et al. 2013; Kurapov & Özkan-Haller 2013; Brodie et al. 2018, 2019; Wilson & Berezhnoy 2018; Collins et al. 2020). So far, data assimilation has been coupled with relatively simple morphological models: Plant & Holland (2011) used a Bayesian approach to assimilate bathymetry, bar location, and wave breaking into a surf-zone wave-propagation model; Vitousek et al. (2017) used an extended Kalman filter to assimilate historical shoreline data into a model for predicting shoreline change; and Ghorbanidehno et al. (2019) demonstrated a fast Kalman filter for assimilating wave data into a bathymetry model. Smith et al. (2009) used a 3D variational assimilation to improve the parameterization of a 1D model of bedform propagation. Scott & Mason (2007) demonstrated improvement in a 2D horizontal (2DH) model of a tidal embayment using data assimilation but noted that both the model and the assimilation methods could be improved.

5.2.6. Ensemble and probabilistic modeling. We predict that ensemble and probabilistic approaches, which are already used in shoreline models (e.g., Montaña et al. 2020), will become more widely used to estimate uncertainties in storm-impact forecasts. Ensemble modeling is one approach for estimating uncertainties. Morphodynamic ensemble modeling of coastal evolution on the decadal scale, such as the MorMerge approach (Roelvink 2006), assumes that conditions can be run in parallel, but this is not yet broadly feasible for the more computationally demanding models applied on the storm-event scale. Instead, recent work has used reduced-complexity hydrodynamic models with simplified physics to rapidly generate a range of input boundary conditions, such as surge simulations with SFINCS (Leijnse et al. 2021). Reduced-complexity models have found more widespread use for timescales of ~10–100 years under sea-level rise (Ranasinghe 2020). Ensemble modeling can also be used to account for the variations in modeled oceanographic forcing and morphodynamic response due to uncertainty in model parameters. By varying the parameters (sediment size, type, and depth; eddy viscosity; the breaker index; the critical Shields parameter; etc.) over a realistic range within the ensemble members, one can output a probabilistic representation of the morphological response for a given domain.

5.2.7. More observations. The greatest uncertainties in initializing, forcing, and validating models of morphodynamic change arise from sparse, missing, or untimely data. While there are an increasing number of remotely sensed coastal observations (e.g., from surf cameras, satellites, and crowdsourced data), some sources of data have not kept pace. The number of long-term coastal observation stations (water-level measurements and offshore buoys) has not increased

significantly, nor has the frequency of topo-bathymetric lidar data acquisition. Although new technology has been developed for measuring nearshore bathymetry (autonomous vessels, autonomous bottom vehicles, bathymetric lidar on unmanned aircraft systems, and inversion from wave information) and surf-zone conditions (visual and infrared imagery, radar, and lidar; Holman & Haller 2013), these methods have not been widely deployed, are expensive, and may not be robust enough to measure during storms. There is, however, a trend toward increased rapid-response measurements, including various National Science Foundation–funded rapid-response projects (Raubenheimer 2020; <https://converge.colorado.edu/research-networks>); expanded emergency-response flights (<https://storms.ngs.noaa.gov>); a recently funded initiative by the US Office of Naval Research (NOPP 2020); operational efforts by the US Federal Emergency Management Agency, US Geological Survey, and US Army Corps of Engineers; and crowdsourced data like CoastSnap (Harley et al. 2019) and the Federal Crowdsourcing and Citizen Science Catalog (<https://www.citizenscience.gov/catalog>). Despite the improvement in rapid-response observations, the overall paucity of data remains the greatest challenge for improving models of morphodynamic responses to extreme events.

DISCLOSURE STATEMENT

The authors are not aware of any affiliations, memberships, funding, or financial holdings that might be perceived as affecting the objectivity of this review.

AUTHOR CONTRIBUTIONS

J.D. contributed to Sections 3.1 and 3.2 and **Figure 2**. C.A.H. contributed to Sections 2.2, 3.3, 3.4, and 4; **Figure 5**; and the **Supplemental Material**. T.-J.H. contributed parts of Sections 3.5 and 5.1. T.S.K. contributed to Sections 3.4–3.6 and created **Figure 4**. M.O. contributed to Sections 1 and 3.3 and edited the manuscript. A.M.P. contributed to Sections 3.6 and 5.2, **Figure 3**, and the **Supplemental Material** and created **Figure 7**. Y.R. contributed to Sections 2.2, 3.4, and 3.5 and **Figure 4**. D.R. contributed to Sections 3.4, 3.5, 3.8, and 3.9. C.R.S. contributed to Sections 1, 2.1, 2.2, 3.4, 3.5, 3.8, 3.9, 4, and 5; modified **Figure 1**; assembled the Literature Cited; and edited the manuscript. M.v.d.L. contributed to Sections 3.6, 3.8, 4, and 5.2; **Figure 6**; and the **Supplemental Material**. A.v.D. contributed to Sections 2.1, 2.2, 3.4, 5.1, and 5.2 and the **Supplemental Material** and edited the manuscript. J.V. contributed to Sections 1, 3.4, and 5 and **Figure 7**. J.C.W. contributed to Sections 2.1, 3.4–3.6, and 3.7.

ACKNOWLEDGMENTS

All authors except D.R. were partially supported by the IFMSIP project, funded by US Office of Naval Research grant PE 0601153N under contracts N00014-17-1-2459 (Deltares), N00014-18-1-2785 (University of Delaware), N0001419WX00733 (US Naval Research Laboratory, Monterey), N0001418WX01447 (US Naval Research Laboratory, Stennis Space Center), and N0001418IP00016 (US Geological Survey). C.R.S., C.A.H., T.S.K., and J.C.W. were supported by the US Geological Survey Coastal/Marine Hazards and Resources Program. A.v.D. and M.v.d.L. were supported by the Deltares Strategic Research project Quantifying Flood Hazards and Impacts. M.O. acknowledges support from National Science Foundation project OCE-1554892. We thank Jim Duncan at Annual Reviews for handling this review and outstanding copyediting, and Glenda Mahoney for editing the figures. Early drafts of this article were greatly improved by comments and suggestions from Meg Palmsten and Sean Vitousek.

LITERATURE CITED

- Abreu T, Silva PA, Sancho F, Temperville A. 2010. Analytical approximate wave form for asymmetric waves. *Coast. Eng.* 57:656–67
- Albatal A, Wadman H, Stark N, Bilici C, McNinch J. 2019. Investigation of spatial and short-term temporal nearshore sandy sediment strength using a portable free fall penetrometer. *Coast. Eng.* 143:21–37
- Alexander PS, Holman RA. 2004. Quantification of nearshore morphology based on video imaging. *Mar. Geol.* 208:101–11
- Amoudry LO, Souza AJ. 2011. Deterministic coastal morphological and sediment transport modeling: a review and discussion. *Rev. Geophys.* 49:RG2002
- Anarde K, Figlus J, Sous D, Tissier M. 2020. Transformation of infragravity waves during hurricane overwash. *J. Mar. Sci. Eng.* 8:545
- Andrews DG, McIntyre ME. 1978. An exact theory of nonlinear waves on a Lagrangian-mean flow. *J. Fluid Mech.* 89:609–46
- Arcemet GJ Jr., Schneider VR. 1989. *Guide for selecting Manning's roughness coefficients for natural channels and flood plains*. Water Supply Pap. 2339, US Geol. Surv., Denver, CO
- Ardhuin F, Gille ST, Menemenlis D, Rocha CB, Rasche N, et al. 2017. Small-scale open ocean currents have large effects on wind wave heights. *J. Geophys. Res. Oceans* 122:4500–17
- Ardhuin F, Rasche N, Belibassakis KA. 2008. Explicit wave-averaged primitive equations using a generalized Lagrangian mean. *Ocean Model.* 20:35–60
- Ashton AD, Murray AB. 2006. High-angle wave instability and emergent shoreline shapes: 1. Modeling of sand waves, flying spits, and capes. *J. Geophys. Res. Earth Surf.* 111:F04011
- Ashton AD, Murray AB, Arnoult O. 2001. Formation of coastline features by large-scale instabilities induced by high-angle waves. *Nature* 414:296–300
- Baar AW, Boechat Albernaz M, van Dijk WM, Kleinhans MG. 2019. Critical dependence of morphodynamic models of fluvial and tidal systems on empirical downslope sediment transport. *Nat. Commun.* 10:4903
- Bailard JA, Inman DL. 1981. An energetics bedload model for a plane sloping beach: local transport. *J. Geophys. Res. Oceans* 86:2035–43
- Bakhtyar R, Maitaria K, Velissariou P, Trimble B, Mashriqui H, et al. 2020. A new 1D/2D coupled modeling approach for a riverine-estuarine system under storm events: application to Delaware River Basin. *J. Geophys. Res. Oceans* 125:e2019JC015822
- Bao J-W, Wilczak JM, Choi J-K, Kantha LH. 2000. Numerical simulations of air-sea interaction under high wind conditions using a coupled model: a study of hurricane development. *Mon. Weather Rev.* 128:2190–210
- Battjes JA, Bakkenes HJ, Janssen TT, van Dongeren AR. 2004. Shoaling of subharmonic gravity waves. *J. Geophys. Res. Oceans* 109:C02009
- Bauer P, Thorpe A, Brunet G. 2015. The quiet revolution of numerical weather prediction. *Nature* 525:47–55
- Baumann J, Chaumillon E, Bertin X, Schneider J-L, Guillot B, Schmutz M. 2017. Importance of infragravity waves for the generation of washover deposits. *Mar. Geol.* 391:20–35
- Bertin X, de Bakker A, van Dongeren A, Coco G, André G, et al. 2018. Infragravity waves: from driving mechanisms to impacts. *Earth-Sci. Rev.* 177:774–99
- Bertin X, Mendes D, Martins K, Fortunato AB, Lavaud L. 2019. The closure of a shallow tidal inlet promoted by infragravity waves. *Geophys. Res. Lett.* 46:6804–10
- Beudin A, Kalra TS, Ganju NK, Warner JC. 2017. Development of a coupled wave-flow-vegetation interaction model. *Comput. Geosci.* 100:76–86
- Billson O, Russell P, Davidson M. 2019. Storm waves at the shoreline: When and where are infragravity waves important? *J. Mar. Sci. Eng.* 7:139
- Birrien F, Castelle B, Marieu V, Dubarrier B. 2013. On a data-model assimilation method to inverse wave-dominated beach bathymetry using heterogeneous video-derived observations. *Ocean Eng.* 73:126–38
- Black PG, D'Asaro EA, Drennan WM, French JR, Niiler PP, et al. 2007. Air-sea exchange in hurricanes: synthesis of observations from the coupled boundary layer air-sea transfer experiment. *Bull. Am. Meteorol. Soc.* 88:357–74

- Blake ES, Kimberlain TB, Berg RJ, Cangialosi JP, Beven JL II. 2013. *Tropical cyclone report: Hurricane Sandy (AL182012), 22–29 October 2012*. Rep., Natl. Hurric. Cent., Miami
- Bosboom J, Reniers AJHM. 2014. Displacement-based error metrics for morphodynamic models. *Adv. Geosci.* 39:37–43
- Bosboom J, Reniers AJHM, Luijendijk AP. 2014. On the perception of morphodynamic model skill. *Coast. Eng.* 94:112–25
- Braun SA, Montgomery MT, Pu Z. 2006. High-resolution simulation of Hurricane Bonnie (1998). Part I: the organization of eyewall vertical motion. *J. Atmos. Sci.* 63:19–42
- Brodie KL, Bruder BL, Slocum RK, Spore NJ. 2019. Simultaneous mapping of coastal topography and bathymetry from a lightweight multicamera UAS. *IEEE Trans. Geosci. Remote Sens.* 57:6844–64
- Brodie KL, Palmsten ML, Hesser TJ, Dickhudt PJ, Raubenheimer B, et al. 2018. Evaluation of video-based linear depth inversion performance and applications using altimeters and hydrographic surveys in a wide range of environmental conditions. *Coast. Eng.* 136:147–60
- Bruun P. 1954. *Coast erosion and the development of beach profiles*. Tech. Memo 44, Beach Eros. Board, US Army Corps Eng., Washington, DC
- Bruun P. 1962. Sea-level rise as a cause of shore erosion. *J. Waterw. Harb. Div.* 88:117–32
- Bryant KM, Akbar M. 2016. An exploration of wind stress calculation techniques in hurricane storm surge modeling. *J. Mar. Sci. Eng.* 4:58
- Buijsman MC, Ruggiero P, Kaminsky GM. 2001. Sensitivity of shoreline change predictions to wave climate variability along the southwest Washington coast, USA. In *Coastal Dynamics '01*, ed. H Hanson, M Larson, pp. 617–26. Reston, VA: Am. Soc. Civil Eng.
- Buscombe D, Ritchie A. 2018. Landscape classification with deep neural networks. *Geosciences* 8:244
- Callaghan DP, Saint-Cast F, Nielsen P, Baldock TE. 2006. Numerical solutions of the sediment conservation law; a review and improved formulation for coastal morphological modelling. *Coast. Eng.* 53:557–71
- Carr JA, D’Odorico P, McGlathery KJ, Wiberg PL. 2012. Modeling the effects of climate change on eelgrass stability and resilience: future scenarios and leading indicators of collapse. *Mar. Ecol. Prog. Ser.* 448:289–301
- Casulli V. 1999. A semi-implicit finite difference method for non-hydrostatic, free-surface flows. *Int. J. Numer. Methods Fluids* 30:425–40
- Cavaleri L, Abdalla S, Benetazzo A, Bertotti L, Bidlot J-R, et al. 2018. Wave modelling in coastal and inner seas. *Prog. Oceanogr.* 167:164–233
- Cavaleri L, Barbariol F, Benetazzo A. 2020. Wind-wave modeling: where we are, where to go. *J. Mar. Sci. Eng.* 8:260
- Chen C, Liu H, Beardsley RC. 2003. An unstructured grid, finite-volume, three-dimensional, primitive equations ocean model: application to coastal ocean and estuaries. *J. Atmos. Ocean. Technol.* 20:159–86
- Chen J-L, Shi F, Hsu T-J, Kirby JT. 2014. NearCoM-TVD—a quasi-3D nearshore circulation and sediment transport model. *Coast. Eng.* 91:200–12
- Chen S, Campbell TJ, Jin H, Gaberšek S, Hodur RM, Martin P. 2010. Effect of two-way air-sea coupling in high and low wind speed regimes. *Mon. Weather Rev.* 138:3579–602
- Chiang Y-C, Hsiao S-S, Lin M-C. 2011. Improved technique for controlling oscillation of coastal morphological modeling system. *J. Mar. Sci. Technol.* 19:625–33
- Cienfuegos R, Barthélemy E, Bonneton P. 2006. A fourth-order compact finite volume scheme for fully nonlinear and weakly dispersive Boussinesq-type equations. Part I: model development and analysis. *Int. J. Numer. Methods Fluids* 51:1217–53
- Cienfuegos R, Barthélemy E, Bonneton P. 2007. A fourth-order compact finite volume scheme for fully nonlinear and weakly dispersive Boussinesq-type equations. Part II: boundary conditions and validation. *Int. J. Numer. Methods Fluids* 53:1423–55
- Coco G, Zhou Z, van Maanen B, Olabarrieta M, Tinoco R, Townend I. 2013. Morphodynamics of tidal networks: advances and challenges. *Mar. Geol.* 346:1–16
- Cohn N, Hoonhout BM, Goldstein EB, de Vries S, Moore LJ, et al. 2019a. Exploring marine and aeolian controls on coastal foredune growth using a coupled numerical model. *J. Mar. Sci. Eng.* 7:13
- Cohn N, Ruggiero P, García-Medina G, Anderson D, Serafin KA, Biel R. 2019b. Environmental and morphologic controls on wave-induced dune response. *Geomorphology* 329:108–28

- Collins AM, Brodie KL, Bak SA, Hesser TJ, Farthing MW, et al. 2020. Bathymetric inversion and uncertainty estimation from synthetic surf-zone imagery with machine learning. *Remote Sens.* 12:3364
- Craik ADD, Leibovich S. 1976. A rational model for Langmuir circulations. *J. Fluid Mech.* 73:401–26
- Curcic M, Haus BK. 2020. Revised estimates of ocean surface drag in strong winds. *Geophys. Res. Lett.* 47:e2020GL087647
- Dalrymple RA, Kirby JT, Hwang PA. 1984. Wave diffraction due to areas of energy dissipation. *J. Waterway Port Coast. Ocean Eng.* 110:67–79
- D’Asaro EA, Black P, Centurioni L, Harr P, Jayne S, et al. 2011. Typhoon-ocean interaction in the western North Pacific: part 1. *Oceanography* 24(4):24–31
- Davidson MA, Lewis RP, Turner IL. 2010. Forecasting seasonal to multi-year shoreline change. *Coast. Eng.* 57:620–29
- Davidson MA, Splinter KD, Turner IL. 2013. A simple equilibrium model for predicting shoreline change. *Coast. Eng.* 73:191–202
- Davidson SG, Hesp PA, da Silva GM. 2020. Controls on dune scarping. *Prog. Phys. Geogr. Earth Environ.* 44:923–47
- Davidson-Arnott R, Bauer B, Houser C. 2019. *Introduction to Coastal Processes and Geomorphology*. Cambridge, UK: Cambridge Univ. Press. 2nd ed.
- Davies AG, Robins PE. 2017. Residual flow, bedforms and sediment transport in a tidal channel modelled with variable bed roughness. *Geomorphology* 295:855–72
- Davis C, Wang W, Chen SS, Chen Y, Corbosiero K, et al. 2008. Prediction of landfalling hurricanes with the Advanced Hurricane WRF model. *Mon. Weather Rev.* 136:1990–2005
- de Ridder MP, Smit PB, van Dongeren AR, McCall RT, Nederhoff K, Reniers AJHM. 2021. Efficient two-layer non-hydrostatic wave model with accurate dispersive behaviour. *Coast. Eng.* 164:103808
- de Swart HE, Zimmerman JTF. 2009. Morphodynamics of tidal inlet systems. *Annu. Rev. Fluid Mech.* 41:203–29
- de Vet PLM, McCall RT, den Bieman JP, Stive MJF, van Ormondt M. 2015. Modelling dune erosion, overwash and breaching at Fire Island (NY) during Hurricane Sandy. In *The Proceedings of the Coastal Sediments 2015*, ed. P Wang, JD Rosati, J Cheng. Singapore: World Sci. https://doi.org/10.1142/9789814689977_0006
- de Vriend HJ, Zyserman J, Nicholson J, Roelvink JA, Péchon P, Southgate HN. 1993. Medium-term 2DH coastal area modelling. *Coast. Eng.* 21:193–224
- Dean RG. 1991. Equilibrium beach profiles: characteristics and applications. *J. Coast. Res.* 7:53–84
- Debreu L, Marchesiello P, Penven P, Cambon G. 2012. Two-way nesting in split-explicit ocean models: algorithms, implementation and validation. *Ocean Model.* 49–50:1–21
- DeMaria M, Mainelli M, Shay LK, Knaff JA, Kaplan J. 2005. Further improvements to the Statistical Hurricane Intensity Prediction Scheme (SHIPS). *Weather Forecast.* 20:531–43
- Dingemans MW. 1997. *Water Wave Propagation Over Uneven Bottoms: Part 1 – Linear Wave Propagation*. Singapore: World Sci.
- Doering JC, Bowen AJ. 1995. Parametrization of orbital velocity asymmetries of shoaling and breaking waves using bispectral analysis. *Coast. Eng.* 26:15–33
- Doering JC, Elfrink B, Hanes DM, Ruessink G. 2000. Parameterization of velocity skewness under waves and its effect on cross-shore sediment transport. *Coast. Eng. Proc.* 27:1383–97
- Doyle JD, Hodur R, Chen S, Jin Y, Msokaitis J, et al. 2014. Tropical cyclone prediction using COAMPS-TC. *Oceanography* 27(3):104–15
- Doyle JD, Jin Y, Hodur RM, Chen S, Jin H, et al. 2012. Real-time tropical cyclone prediction using COAMPS-TC. *Adv. Geosci.* 28:15–28
- Drake TG, Calantoni J. 2001. Discrete particle model for sheet flow sediment transport in the nearshore. *J. Geophys. Res. Oceans* 106:19859–68
- Drost EJJ, Cuttler MVW, Lowe RJ, Hansen JE. 2019. Predicting the hydrodynamic response of a coastal reef-lagoon system to a tropical cyclone using phase-averaged and surfbeat-resolving wave models. *Coast. Eng.* 152:103525
- Durán O, Moore LJ. 2013. Vegetation controls on the maximum size of coastal dunes. *PNAS* 110:17217–22

- Elgar S, Guza RT. 1985. Observations of bispectra of shoaling surface gravity waves. *J. Fluid Mech.* 161:425–48
- Exner FM. 1920. Zur Physik der Dünen. *Akad. Wiss. Wien Math. Naturwiss. Klasse* 129:929–52
- Exner FM. 1925. Über die Wechselwirkung zwischen Wasser und Geschiebe in Flüssen. *Akad. Wiss. Wien Math. Naturwiss. Klasse* 135:165–204
- Ezer T, Atkinson LP, Tuleya R. 2017. Observations and operational model simulations reveal the impact of Hurricane Matthew (2016) on the Gulf Stream and coastal sea level. *Dyn. Atmos. Oceans* 80:124–38
- Fairall CW, Banner ML, Peirson WL, Asher W, Morison RP. 2009. Investigation of the physical scaling of sea spray spume droplet production. *J. Geophys. Res. Oceans* 114:C10001
- Fernández-Mora A, Calvete D, Falqués A, de Swart HE. 2015. Onshore sandbar migration in the surf zone: new insights into the wave-induced sediment transport mechanisms. *Geophys. Res. Lett.* 42:2869–77
- Ferreira CM, Irish JL, Olivera F. 2014. Uncertainty in hurricane surge simulation due to land cover specification. *J. Geophys. Res. Oceans* 119:1812–27
- Foda MA, Mei CC. 1981. Nonlinear excitation of long-trapped waves by a group of short swells. *J. Fluid Mech.* 111:319–45
- Foster DL, Bowen AJ, Holman RA, Nattoo P. 2006. Field evidence of pressure gradient induced incipient motion. *J. Geophys. Res. Oceans* 111:C05004
- Fringer OB, Dawson CN, He R, Ralston DK, Zhang YJ. 2019. The future of coastal and estuarine modeling: findings from a workshop. *Ocean Model.* 143:101458
- Fringer OB, Gerritsen M, Street RL. 2006. An unstructured-grid, finite-volume, nonhydrostatic, parallel coastal ocean simulator. *Ocean Model.* 14:139–73
- Fuhrman DR, Schløer S, Sterner J. 2013. RANS-based simulation of turbulent wave boundary layer and sheet-flow sediment transport processes. *Coast. Eng.* 73:151–66
- Galappatti G, Vreugdenhil CB. 1985. A depth-integrated model for suspended sediment transport. *J. Hydraul. Res.* 23:359–77
- Gallagher EL, Elgar S, Guza RT. 1998. Observations of sand bar evolution on a natural beach. *J. Geophys. Res. Oceans* 103:3203–15
- Ganju NK, Lentz SJ, Kirincich AR, Farrar JT. 2011. Complex mean circulation over the inner shelf south of Martha's Vineyard revealed by observations and a high-resolution model. *J. Geophys. Res. Oceans* 116:C10036
- Ghorbanidehno H, Lee J, Farthing M, Hesser T, Kitanidis PK, Darve EF. 2019. Novel data assimilation algorithm for nearshore bathymetry. *J. Atmos. Ocean. Technol.* 36:699–715
- Ginis I, Chen X, Hara T. 2021. *Impact of shoaling waves on wind stress and drag coefficient during tropical cyclone landfall*. Paper presented at the 34th Conference on Hurricanes and Tropical Meteorology, virtual, May 10–14
- Goerss JS. 2007. Prediction of consensus tropical cyclone track forecast error. *Mon. Weather Rev.* 135:1985–93
- Goff JA, Allison MA, Gulick SPS. 2010. Offshore transport of sediment during cyclonic storms: Hurricane Ike (2008), Texas Gulf Coast, USA. *Geology* 38:351–54
- Goff JA, Swartz JM, Gulick SPS, Dawson CN, de Alegria-Arzaburu AR. 2019. An outflow event on the left side of Hurricane Harvey: erosion of barrier sand and seaward transport through Aransas Pass, Texas. *Geomorphology* 334:44–57
- Gori A, Lin N, Smith J. 2020. Assessing compound flooding from landfalling tropical cyclones on the North Carolina coast. *Water Resour. Res.* 56:e2019WR026788
- Gorlay MR. 1968. *Beach and dune erosion tests*. Rep. M935/M936, Delft Hydraul. Lab., Delft, Neth.
- Goslin J, Clemmensen LB. 2017. Proxy records of Holocene storm events in coastal barrier systems: storm-wave induced markers. *Quat. Sci. Rev.* 174:80–119
- Grant WD, Madsen OS. 1979. Combined wave and current interaction with a rough bottom. *J. Geophys. Res. Oceans* 84:1797–808
- Hamill TM, Whitaker JS, Kleist DT, Fiorino M, Benjamin SG. 2011. Predictions of 2010's tropical cyclones using the GFS and ensemble-based data assimilation methods. *Mon. Weather Rev.* 139:3243–47
- Han J, Huang L. 2018. Numerical experiments on stagnation points influenced by the Three Gorges Dam in the Yangtze Estuary. *Water Supply* 18:1032–40
- Hapke CJ, Nelson TR, Henderson RE, Brenner OT, Miselis JL. 2017. *Morphologic evolution of the wilderness area breach at Fire Island, New York—2012–15*. Open-File Rep. 2017-1116, US Geol. Surv., Reston, VA

- Harley MD, Kinsela MA, Sánchez-García E, Vos K. 2019. Shoreline change mapping using crowd-sourced smartphone images. *Coast. Eng.* 150:175–89
- Hartanto IM, Beevers L, Popescu I, Wright NG. 2011. Application of a coastal modelling code in fluvial environments. *Environ. Model. Softw.* 26:1685–95
- Harter C, Figlus J. 2017. Numerical modeling of the morphodynamic response of a low-lying barrier island beach and foredune system inundated during Hurricane Ike using XBeach and CSHORE. *Coast. Eng.* 120:64–74
- Hegermiller CA, Warner JC, Olabarrieta M, Sherwood CR. 2019. Wave-current interaction between Hurricane Matthew wave fields and the Gulf Stream. *J. Phys. Oceanogr.* 49:2883–900
- Hemminga MA, Duarte CM. 2000. *Seagrass Ecology*. Cambridge, UK: Cambridge Univ. Press
- Henderson SM, Bowen AJ. 2002. Observations of surf beat forcing and dissipation. *J. Geophys. Res. Oceans* 107:14-1–10
- Héquette A, Ruz M-H, Zemmour A, Marin D, Cartier A, Sipka V. 2019. Alongshore variability in coastal dune erosion and post-storm recovery, northern coast of France. *J. Coast. Res. Spec. Issue* 88:25–45
- Herbers THC, Elgar S, Guza RT. 1994. Infragravity-frequency (0.005–0.05 Hz) motions on the shelf. Part I: forced waves. *J. Phys. Oceanogr.* 24:917–27
- Hervouet J-M. 2007. *Hydrodynamics of Free Surface Flows: Modelling with the Finite Element Method*. West Sussex, UK: Wiley & Sons
- Hoefel F, Elgar S. 2003. Wave-induced sediment transport and sandbar migration. *Science* 299:1885–87
- Holman R, Haller MC. 2013. Remote sensing of the nearshore. *Annu. Rev. Mar. Sci.* 5:95–113
- Holman R, Plant N, Holland T. 2013. cBathy: a robust algorithm for estimating nearshore bathymetry. *J. Geophys. Res. Oceans* 118:2595–609
- Holthuijsen LH. 2007. *Waves in Oceanic and Coastal Waters*. Cambridge, UK: Cambridge Univ. Press
- Holthuijsen LH, Tolman HL. 1991. Effects of the Gulf Stream on ocean waves. *J. Geophys. Res. Oceans* 96:12755–71
- Hoonhout BM, de Vries S. 2016. A process-based model for aeolian sediment transport and spatiotemporal varying sediment availability. *J. Geophys. Res. Earth Surf.* 121:1555–75
- Housego R, Raubenheimer B, Elgar S, Gorrell L, Wadman H, et al. 2018. Barrier Island groundwater. *Coast. Eng. Proc.* 36:risk.10
- Hsu T-J, Elgar S, Guza RT. 2006. Wave-induced sediment transport and onshore sandbar migration. *Coast. Eng.* 53:817–24
- Hsu T-J, Hanes DM. 2004. Effects of wave shape on sheet flow sediment transport. *J. Geophys. Res. Oceans* 109:C05025
- Huizer S, Radermacher M, de Vries S, Oude Essink GHP, Bierkens MFP. 2018. Impact of coastal forcing and groundwater recharge on the growth of a fresh groundwater lens in a mega-scale beach nourishment. *Hydrol. Earth Syst. Sci.* 22:1065–80
- Isobe M, Horikawa K. 1982. Study on water particle velocities of shoaling and breaking waves. *Coast. Eng. Jpn.* 25:109–23
- Janssen TT, Battjes JA, van Dongeren AR. 2003. Long waves induced by short-wave groups over a sloping bottom. *J. Geophys. Res. Oceans* 108:3252
- Johnson HK, Zyserman JA. 2002. Controlling spatial oscillations in bed level update schemes. *Coast. Eng.* 46:109–26
- Kaergaard K, Fredsoe J. 2013. A numerical shoreline model for shorelines with large curvature. *Coast. Eng.* 74:19–32
- Kalra TS, Sherwood CR, Warner JC, Rafati Y, Hsu T-J. 2019. Investigating bedload transport under asymmetrical waves using a coupled ocean-wave model. In *Coastal Sediments 2019*, ed. P Wang, JD Rosati, M Vallee, pp. 591–604. Singapore: World Sci. https://doi.org/10.1142/9789811204487_0052
- Kaveh K, Reisenbüchler M, Lamichhane S, Liepert T, Nguyen ND, et al. 2019. A comparative study of comprehensive modeling systems for sediment transport in a curved open channel. *Water* 11:1779
- Kennedy AB, Gravois U, Zachry BC, Westerink JJ, Hope ME, et al. 2011. Origin of the Hurricane Ike fore-runner surge. *Geophys. Res. Lett.* 38:L08608

- Kim Y, Cheng Z, Hsu T-J, Chauchat J. 2018. A numerical study of sheet flow under monochromatic nonbreaking waves using a free surface resolving eulerian two-phase flow model. *J. Geophys. Res. Oceans* 123:4693–719
- Kim Y, Mieras RS, Cheng Z, Anderson D, Hsu T-J, et al. 2019. A numerical study of sheet flow driven by velocity and acceleration skewed near-breaking waves on a sandbar using SedWaveFoam. *Coast. Eng.* 152:103526
- Kombiadou K, Costas S, Roelvink D. 2021. Simulating destructive and constructive morphodynamic processes in steep beaches. *J. Mar. Sci. Eng.* 9:86
- Kranenburg WM, Ribberink JS, Schretlen JJLM, Uittenbogaard RE. 2013. Sand transport beneath waves: the role of progressive wave streaming and other free surface effects. *J. Geophys. Res. Earth Surf.* 118:122–39
- Kranenburg WM, Ribberink JS, Uittenbogaard RE, Hulscher SJMH. 2012. Net currents in the wave bottom boundary layer: on waveshape streaming and progressive wave streaming. *J. Geophys. Res. Earth Surf.* 117:F03005
- Kumar N, Voulgaris G, Warner JC, Olabarrieta M. 2012. Implementation of the vortex force formalism in the coupled ocean-atmosphere-wave-sediment transport (COAWST) modeling system for inner shelf and surf zone applications. *Ocean Model.* 47(Suppl. C):65–95
- Kurapov AL, Özkan-Haller HT. 2013. Bathymetry correction using an adjoint component of a coupled nearshore wave-circulation model: tests with synthetic velocity data. *J. Geophys. Res. Oceans* 118:4673–88
- Lai Z, Chen C, Cowles GW, Beardsley RC. 2010. A nonhydrostatic version of FVCOM: 1. validation experiments. *J. Geophys. Res. Oceans* 115:C11010
- Lane EM, Restrepo JM, McWilliams JC. 2007. Wave-current interaction: a comparison of radiation-stress and vortex-force representations. *J. Phys. Oceanogr.* 37:1122–41
- Larson M, Hanson H, Kraus NC. 1997. Analytical solutions of one-line model for shoreline change near coastal structures. *J. Waterw. Port Coast. Ocean Eng.* 123:180–91
- Lazarus ED, Goldstein EB. 2019. Is there a bulldozer in your model? *J. Geophys. Res. Earth Surf.* 124:696–99
- Leijnse T, van Ormondt M, Nederhoff K, van Dongeren A. 2021. Modeling compound flooding in coastal systems using a computationally efficient reduced-physics solver: including fluvial, pluvial, tidal, wind- and wave-driven processes. *Coast. Eng.* 163:103796
- Lennon G. 1991. The nature and causes of hurricane-induced ebb scour channels on a developed shoreline. *J. Coast. Res. Spec. Issue* 8:237–48
- Lesser GR, Roelvink JA, van Kester JATM, Stelling GS. 2004. Development and validation of a three-dimensional morphological model. *Coast. Eng.* 51:883–915
- Li M, Li W, Xie M, Xu T. 2020. Morphodynamic responses to the Hong Kong–Zhuhai–Macao Bridge in the Pearl River estuary, China. *J. Coast. Res.* 37:168–78
- List JH. 1992. A model for the generation of two-dimensional surf beat. *J. Geophys. Res. Oceans* 97:5623–35
- Long JW, Plant NG. 2012. Extended Kalman Filter framework for forecasting shoreline evolution. *Geophys. Res. Lett.* 39:L13603
- Longuet-Higgins MS. 2005. On wave set-up in shoaling water with a rough sea bed. *J. Fluid Mech.* 527:217–34
- Longuet-Higgins MS, Stewart RW. 1962. Radiation stress and mass transport in gravity waves, with application to ‘surf beats.’ *J. Fluid Mech.* 13:481–504
- Longuet-Higgins MS, Stewart RW. 1964. Radiation stresses in water waves; a physical discussion, with applications. *Deep-Sea Res. Oceanogr. Abstr.* 11:529–62
- Luhar M, Coutu S, Infantes E, Fox S, Nepf H. 2010. Wave-induced velocities inside a model seagrass bed. *J. Geophys. Res. Oceans* 115:C12005
- Luhar M, Nepf HM. 2011. Flow-induced reconfiguration of buoyant and flexible aquatic vegetation. *Limnol. Oceanogr.* 56:2003–17
- Luijendijk AP, de Schipper MA, Ranasinghe R. 2019. Morphodynamic acceleration techniques for multi-timescale predictions of complex sandy interventions. *J. Mar. Sci. Eng.* 7:78

- Luijendijk AP, Hagenaars G, Ranasinghe R, Baart F, Donchyts G, Aarninkhof S. 2018. The state of the world's beaches. *Sci. Rep.* 8:6641
- Ma G, Kirby JT, Shi F. 2014. *Non-Hydrostatic Wave Model NHWAVE: documentation and user's manual (version 2.0)*. Res. Rep. CACR-14-11, Cent. Appl. Coast. Res., Univ. Del., Newark
- Machineni N, Sinha VSP, Singh P, Reddy NT. 2019. The impact of distributed landuse information in hydrodynamic model application in storm surge inundation. *Estuar. Coast. Shelf Sci.* 231:106466
- MacMahan JH, Thornton EB, Reniers AJHM. 2006. Rip current review. *Coast. Eng.* 53:191–208
- Malej M, Smith JM, Salgado-Dominguez G. 2015. *Introduction to phase-resolving wave modeling with FUNWAVE*. Rep. ERDC/CHL CHETN-I-87, Eng. Res. Dev. Cent., US Army Corps Eng., Vicksburg, MS
- Marks FD, Shay LK. 1998. Landfalling tropical cyclones. *Bull. Am. Meteorol. Soc.* 79:305–23
- Marshall J, Adcroft A, Hill C, Perelman L, Heisey C. 1997. A finite-volume, incompressible Navier Stokes model for studies of the ocean on parallel computers. *J. Geophys. Res. Oceans* 102:5753–66
- Masselink G. 1995. Group bound long waves as a source of infragravity energy in the surf zone. *Cont. Shelf Res.* 15:1525–47
- Mattocks C, Forbes C. 2008. A real-time, event-triggered storm surge forecasting system for the state of North Carolina. *Ocean Model.* 25:95–119
- McWilliams JC, Restrepo JM, Lane EM. 2004. An asymptotic theory for the interaction of waves and currents in coastal waters. *J. Fluid Mech.* 511:135–78
- Mei W, Pasquero C, Primeau F. 2012. The effect of translation speed upon the intensity of tropical cyclones over the tropical ocean. *Geophys. Res. Lett.* 39:L07801
- Mendez FJ, Losada IJ. 2004. An empirical model to estimate the propagation of random breaking and non-breaking waves over vegetation fields. *Coast. Eng.* 51:103–18
- Mendoza A, Abad JD, Langendoen EJ, Wang D, Tassi P, Abderrezzak KEK. 2017. Effect of sediment transport boundary conditions on the numerical modeling of bed morphodynamics. *J. Hydraul. Eng.* 143:04016099
- Mercer D, Sheng J, Greatbatch RJ, Bobanović J. 2002. Barotropic waves generated by storms moving rapidly over shallow water. *J. Geophys. Res. Oceans* 107:16–1–17
- Miller JK, Dean RG. 2004. A simple new shoreline change model. *Coast. Eng.* 58:531–56
- Montaño J, Coco G, Antolínez JAA, Beuzen T, Bryan KR, et al. 2020. Blind testing of shoreline evolution models. *Sci. Rep.* 10:2137
- Moon I-J, Kwon J-I, Lee J-C, Shim J-S, Kang SK, et al. 2009. Effect of the surface wind stress parameterization on the storm surge modeling. *Ocean Model.* 29:115–27
- Morgan JA, Kumar N, Horner-Devine AR, Ahrendt S, Istanbuloglu E, Bandaragoda C. 2020. The use of a morphological acceleration factor in the simulation of large-scale fluvial morphodynamics. *Geomorphology* 356:107088
- Munk WH. 1949. Surf beats. *Eos Trans. AGU* 30:849–54
- Murray AB. 2003. Contrasting the goals, strategies, and predictions associated with simplified numerical models and detailed simulations. In *Prediction in Geomorphology*, ed. PR Wilcock, RM Iverson, pp. 151–65. Washington, DC: Am. Geophys. Union
- Murray AB. 2007. Reducing model complexity for explanation and prediction. *Geomorphology* 90:178–91
- Murray AB, Thieler ER. 2004. A new hypothesis and exploratory model for the formation of large-scale inner-shelf sediment sorting and “rippled scour depressions.” *Cont. Shelf Res.* 24:295–315
- Natl. Hurric. Cent. 2020. National Hurricane Center forecast verification. *National Hurricane Center*. <https://www.nhc.noaa.gov/verification/verify5.shtml>
- Nepf HM. 2012. Flow and transport in regions with aquatic vegetation. *Annu. Rev. Fluid Mech.* 44:123–42
- Nguyen DT, Jacobsen NG, Roelvink D. 2021. Development and validation of quasi-Eulerian mean three-dimensional equations of motion using the generalized Lagrangian mean method. *J. Mar. Sci. Eng.* 9:76
- Nicholson J, Broker I, Roelvink JA, Price D, Tanguy JM, Moreno L. 1997. Intercomparison of coastal area morphodynamic models. *Coast. Eng.* 31:97–123
- Nielsen P. 1992. *Coastal Bottom Boundary Layers and Sediment Transport*. Singapore: World Sci.
- Nielsen P. 2006. Sheet flow sediment transport under waves with acceleration skewness and boundary layer streaming. *Coast. Eng.* 53:749–58

- NOPP (Natl. Oceanogr. Partnersh. Program). 2020. *Predicting Hurricane Coastal Impacts, FY21-24 (CLOSED)*. Fund. Announc., NOPP, Washington, DC. <https://www.nopp.org/2020/predicting-hurricane-coastal-impacts-fy21-24>
- Norheim CA, Herbers THC, Elgar S. 1998. Nonlinear evolution of surface wave spectra on a beach. *J. Phys. Oceanogr.* 28:1534-51
- Olabarrieta M, Valle-Levinson A, Martinez CJ, Pattiaratchi C, Shi L. 2017. Meteotsunamis in the northeastern Gulf of Mexico and their possible link to El Niño Southern Oscillation. *Nat. Hazards* 88:1325-46
- Olabarrieta M, Warner JC, Armstrong B, Zambon JB, He R. 2012. Ocean-atmosphere dynamics during Hurricane Ida and Nor'Ida: an application of the coupled ocean-atmosphere-wave-sediment transport (COAWST) modeling system. *Ocean Model.* 43-44:112-37
- Over J-SR, Brown JA, Sherwood CR, Hegermiller CA, Wernette PA, et al. 2021. A survey of storm-induced seaward-transport features observed during the 2019 and 2020 hurricane seasons. *Shore Beach* 89(2):31-40
- Overton MF, Fisher JS. 1988. Simulation modeling of dune erosion. *Coast. Eng. Proc.* 28:1857-67
- Palmsten ML, Holman RA. 2011. Infiltration and instability in dune erosion. *J. Geophys. Res. Oceans* 116:C10030
- Paola C, Voller VR. 2005. A generalized Exner equation for sediment mass balance. *J. Geophys. Res. Earth Surf.* 110:F04014
- Pelnaud-Considère R. 1957. Essai de théorie de l'évolution des formes de rivage en plages de sable et de galets. In *Les Énergies de la Mer: Compte Rendu des Quatrièmes Journées de l'Hydraulique; Paris 13, 14 et 15 Juin 1956*, Vol. 1, pp. 289-301. Paris: Soc. Hydrotech. Fr.
- Plant NG, Holland KT. 2011. Prediction and assimilation of surf-zone processes using a Bayesian network: part II: inverse models. *Coast. Eng.* 58:256-66
- Ponte RM. 1992. The sea level response of a stratified ocean to barometric pressure forcing. *J. Phys. Oceanogr.* 22:109-13
- Pringle WJ, Gonzalez-Lopez J, Joyce BR, Westerink JJ, van der Westhuysen AJ. 2019. Baroclinic coupling improves depth-integrated modeling of coastal sea level variations around Puerto Rico and the U.S. Virgin Islands. *J. Geophys. Res. Oceans* 124:2196-217
- Rafati Y, Hsu T-J, Elgar S, Raubenheimer B, Quataert E, van Dongeren A. 2021. Modeling the hydrodynamics and morphodynamics of sandbar migration events. *Coast. Eng.* 166:103885
- Ranasinghe R. 2020. On the need for a new generation of coastal change models for the 21st century. *Sci. Rep.* 10:2010
- Ranasinghe R, Swinkels C, Luijendijk A, Roelvink D, Bosboom J, et al. 2011. Morphodynamic upscaling with the MORFAC approach: dependencies and sensitivities. *Coast. Eng.* 58:806-11
- Rapizo H, Durrant TH, Babanin AV. 2018. An assessment of the impact of surface currents on wave modeling in the Southern Ocean. *Ocean Dyn.* 68:939-55
- Raubenheimer B. 2020. Development of a nearshore extreme events reconnaissance community. *Coast. Eng. Proc.* 36:keynote.12
- Reniers AJHM, Gallagher EL, MacMahan JH, Brown JA, van Rooijen AA, et al. 2013. Observations and modeling of steep-beach grain-size variability. *J. Geophys. Res. Oceans* 118:577-91
- Rey AJM, Corbett DR, Mulligan RP. 2020. Impacts of hurricane winds and precipitation on hydrodynamics in a back-barrier estuary. *J. Geophys. Res. Oceans* 125:e2020JC016483
- Ribberink JS, van der A DA, Buijsrogge RH. 2010. *SANTOSS transport model: a new formula for sand transport under waves and currents*. Rep. SANTOSS_UT_IR3, Univ. Twente, Twente, Neth.
- Rienecker MM, Fenton JD. 1981. A Fourier approximation method for steady water waves. *J. Fluid Mech.* 104:119-37
- Rocha MVL, Michallet H, Silva PA. 2017. Improving the parameterization of wave nonlinearities – the importance of wave steepness, spectral bandwidth and beach slope. *Coast. Eng.* 121:77-89
- Roelvink D, Costas S. 2019. Coupling nearshore and aeolian processes: XBeach and Duna process-based models. *Environ. Model. Softw.* 115:98-112
- Roelvink D, McCall R, Costas S, van der Lugt M. 2019. Controlling swash zone slope is key to beach profile modelling. In *Coastal Sediments 2019*, ed. P Wang, JD Rosati, M Válee, pp. 149-57. Singapore: World Sci.

- Roelvink D, Reniers A. 2012. *A Guide to Modeling Coastal Morphology*. Singapore: World Sci.
- Roelvink D, Reniers A, van Dongeren A, van Thiel de Vries J, McCall R, Lescinski J. 2009. Modelling storm impacts on beaches, dunes and barrier islands. *Coast. Eng.* 56:1133–52
- Roelvink JA. 2006. Coastal morphodynamic evolution techniques. *Coast. Eng.* 53:277–87
- Roelvink JA, Broker I. 1993. Cross-shore profile models. *Coast. Eng.* 21:163–91
- Roelvink JA, Stive MJF. 1989. Bar-generating cross-shore flow mechanisms on a beach. *J. Geophys. Res. Oceans* 94:4785–800
- Roelvink JA, van Banning GKFM. 1995. Design and development of DELFT3D and application to coastal morphodynamics. *Oceanogr. Lit. Rev.* 11:925
- Rogers R, Aberson S, Black M, Black P, Cione J, et al. 2006. The Intensity Forecasting Experiment: a NOAA multiyear field program for improving tropical cyclone intensity forecasts. *Bull. Am. Meteorol. Soc.* 87:1523–38
- Romero L, Hypolite D, McWilliams JC. 2020. Submesoscale current effects on surface waves. *Ocean Model.* 153:101662
- Ruessink BG, Ramaekers G, van Rijn LC. 2012. On the parameterization of the free-stream non-linear wave orbital motion in nearshore morphodynamic models. *Coast. Eng.* 65:56–63
- Safak I, List JH, Warner JC, Schwab WC. 2017. Persistent shoreline shape induced from offshore geologic framework: effects of shoreface connected ridges. *J. Geophys. Res. Oceans* 122:8721–38
- Sallenger AH Jr. 2000. Storm impact scale for barrier islands. *J. Coast. Res.* 16:890–95
- Santiago-Collazo FL, Bilskie MV, Hagen SC. 2019. A comprehensive review of compound inundation models in low-gradient coastal watersheds. *Environ. Model. Softw.* 119:166–81
- Schäffer HA, Svendsen IA. 1988. Surf beat generation on a mild-slope beach. *Coast. Eng. Proc.* 21:1058–72
- Schambach L, Grilli AR, Grilli ST, Hashemi MR, King JW. 2018. Assessing the impact of extreme storms on barrier beaches along the Atlantic coastline: application to the southern Rhode Island coast. *Coast. Eng.* 133:26–42
- Schoonees JS, Theron AK. 1995. Evaluation of 10 cross-shore sediment transport/morphological models. *Coast. Eng.* 25:1–41
- Schweiger C, Kaehler C, Koldrack N, Schuettrumpf H. 2020. Spatial and temporal evaluation of storm-induced erosion modelling based on a two-dimensional field case including an artificial unvegetated research dune. *Coast. Eng.* 161:103752
- Scott TR, Mason DC. 2007. Data assimilation for a coastal area morphodynamic model: Morecambe Bay. *Coast. Eng.* 54:91–109
- Sherman DJ, Hales BU, Potts MK, Ellis JT, Liu H, Houser C. 2013. Impacts of Hurricane Ike on the beaches of the Bolivar Peninsula, TX, USA. *Geomorphology* 199:62–81
- Sherwood CR, Harris CK, Geyer WR, Butman B. 2002. Toward a community coastal sediment transport modeling system: the second workshop. *Eos Trans. AGU* 83:604
- Sherwood CR, Signell RP, Harris CK, Butman B. 2000. Workshop discusses community models for coastal sediment transport. *Eos Trans. AGU* 81:502
- Sherwood CR, Warrick JA, Hill AD, Ritchie AC, Andrews BD, Plant NG. 2018. Rapid, remote assessment of Hurricane Matthew impacts using four-dimensional structure-from-motion photogrammetry. *J. Coast. Res.* 34:1303–16
- Shi L, Olabarrieta M, Nolan DS, Warner JC. 2020. Tropical cyclone rainbands can trigger meteotsunamis. *Nat. Commun.* 11:678
- Siviglia A, Crosato A. 2016. Numerical modelling of river morphodynamics: latest developments and remaining challenges. *Adv. Water Resour.* 93:1–3
- Smallegan SM, Irish JL, van Dongeren AR, den Bieman JP. 2016. Morphological response of a sandy barrier island with a buried seawall during Hurricane Sandy. *Coast. Eng.* 110:102–10
- Smit P, Janssen T, Holthuijsen L, Smith J. 2014. Non-hydrostatic modeling of surf zone wave dynamics. *Coast. Eng.* 83:36–48
- Smith JD. 1977. Modeling of sediment transport on continental shelves. In *The Sea*, Vol. 6: *Marine Modeling*, ed. ED Goldberg, IN McCave, JJ O'Brien, JH Steele, pp. 539–77. New York: Wiley-Intersci.
- Smith PJ, Dance SL, Baines MJ, Nichols NK, Scott TR. 2009. Variational data assimilation for parameter estimation: application to a simple morphodynamic model. *Ocean Dyn.* 59:697

- Soulsby RL. 1997. *Dynamics of Marine Sands*. London: Telford
- Splinter KD, Carley JT, Golshani A, Tomlinson R. 2014. A relationship to describe the cumulative impact of storm clusters on beach erosion. *Coast. Eng.* 83:49–55
- Stark N, McNinch J, Wadman H, Graber HC, Albatal A, Mallas PA. 2017. Friction angles at sandy beaches from remote imagery. *Géotech. Lett.* 7:292–97
- Stelling GS, Duijnmeijer SPA. 2003. A staggered conservative scheme for every Froude number in rapidly varied shallow water flows. *Int. J. Numer. Methods Fluids* 43:1329–54
- Stockdon HF, Holman RA. 2000. Estimation of wave phase speed and nearshore bathymetry from video imagery. *J. Geophys. Res. Oceans* 105:22015–33
- Stockdon HF, Holman RA, Howd PA, Sallenger AH. 2006. Empirical parameterization of setup, swash, and runup. *Coast. Eng.* 53:573–88
- Stow CA, Jolliff J, McGillicuddy DJ, Doney SC, Allen JI, et al. 2009. Skill assessment for coupled biological/physical models of marine systems. *J. Mar. Syst.* 76:4–15
- Sutherland J, Peet AH, Soulsby RL. 2004. Evaluating the performance of morphological models. *Coast. Eng.* 51:917–39
- Suzuki T, Zijlema M, Burger B, Meijer MC, Narayan S. 2012. Wave dissipation by vegetation with layer schematization in SWAN. *Coast. Eng.* 59:64–71
- Svendsen IA. 2006. *Introduction to Nearshore Hydrodynamics*. Singapore: World Sci.
- Symonds G, Huntley DA, Bowen AJ. 1982. Two-dimensional surfbeat: long wave generation by a time-varying breakpoint. *J. Geophys. Res. Oceans* 87:492–98
- Tassi P, Villaret C. 2014. *Sisyphe v6.3 user manual*. User Man. H-P74-2012-02004-EN, Electr. Fr. Res. Dev., Chatou
- Tavakkol S, Lynett P. 2017. Celeris: a GPU-accelerated open source software with a Boussinesq-type wave solver for real-time interactive simulation and visualization. *Comput. Phys. Commun.* 217:117–27
- Tissier M, Bonneton P, Marche F, Chazel F, Lannes D. 2011. Nearshore dynamics of tsunami-like undular bores using a fully nonlinear Boussinesq model. *J. Coast. Res. Spec. Issue* 64:603–7
- Tissier M, Bonneton P, Michallet H, Ruessink BG. 2015. Infragravity-wave modulation of short-wave celerity in the surf zone. *J. Geophys. Res. Oceans* 120:6799–814
- Tucker MJ. 1950. Surf beats: sea waves of 1 to 5 min. period. *Proc. R. Soc. Lond. A* 202:565–73
- Uchiyama Y, McWilliams JC, Shchepetkin AF. 2010. Wave-current interaction in an oceanic circulation model with a vortex-force formalism: application to the surf zone. *Ocean Model.* 34:16–35
- Uittenbogaard R. 2003. *Modelling turbulence in vegetated aquatic flows*. Paper presented at the International Workshop on Riparian Forest Vegetated Channels: Hydraulic, Morphological and Ecological Aspects, Trento, It., Feb. 20–22
- van der A DA, Ribberink JS, van der Werf JJ, O’Donoghue T, Buijsrogge RH, Kranenburg WM. 2013. Practical sand transport formula for non-breaking waves and currents. *Coast. Eng.* 76:26–42
- van der Lugt MA, Quataert E, van Dongeren A, van Ormondt M, Sherwood CR. 2019. Morphodynamic modeling of the response of two barrier islands to Atlantic hurricane forcing. *Estuar. Coast. Shelf Sci.* 229:106404
- van der Wegen M, Roelvink JA. 2008. Long-term morphodynamic evolution of a tidal embayment using a two-dimensional, process-based model. *J. Geophys. Res. Oceans* 113:C03016
- van Dongeren AR, Battjes J, Janssen T, van Noorloos J, Steenhauer K, et al. 2007. Shoaling and shoreline dissipation of low-frequency waves. *J. Geophys. Res. Oceans* 112:C02011
- van Dongeren AR, Plant N, Cohen A, Roelvink D, Haller MC, Catalán P. 2008. Beach Wizard: nearshore bathymetry estimation through assimilation of model computations and remote observations. *Coast. Eng.* 55:1016–27
- van Dongeren AR, Reniers A, Battjes J, Svendsen I. 2003. Numerical modeling of infragravity wave response during DELILAH. *J. Geophys. Res. Oceans* 108:3288
- van Gent MRA. 2001. Wave runup on dikes with shallow foreshores. *J. Water. Port Coast. Ocean Eng.* 127:254–62
- van Ormondt M, Nelson TR, Hapke CJ, Roelvink D. 2020. Morphodynamic modelling of the wilderness breach, Fire Island, New York. Part I: model set-up and validation. *Coast. Eng.* 157:103621

- van Rijn LC. 2007a. Unified view of sediment transport by currents and waves. I: initiation of motion, bed roughness, and bed-load transport. *J. Hydraul. Eng.* 133:649–67
- van Rijn LC. 2007b. Unified view of sediment transport by currents and waves. II: suspended transport. *J. Hydraul. Eng.* 133:668–89
- van Rijn LC, Walstra DJR, Grasmeijer B, Sutherland J, Pan S, Sierra JP. 2003. The predictability of cross-shore bed evolution of sandy beaches at the time scale of storms and seasons using process-based Profile models. *Coast. Eng.* 47:295–327
- van Rooijen AA, McCall RT, van Thiel de Vries JSM, van Dongeren AR, Reniers AJHM, Roelvink JA. 2016. Modeling the effect of wave-vegetation interaction on wave setup. *J. Geophys. Res. Oceans* 121:4341–59
- van Thiel de Vries JSM, van Gent MRA, Walstra DJR, Reniers AJHM. 2008. Analysis of dune erosion processes in large-scale flume experiments. *Coast. Eng.* 55:1028–40
- Vetsch D, Rousselot P, Volz C, Vonwiller L, Peter S, et al. 2014. *System manuals of BASEMENT: version 2.4*. User Man., Lab. Hydraul., Glaciol., Hydrol., ETH Zurich, Zurich
- Visser PJ. 1994. A model for breach growth in sand-dikes. *Coast. Eng. Proc.* 24:2755–69
- Vitousek S, Barnard PL, Limber P, Erikson L, Cole B. 2017. A model integrating longshore and cross-shore processes for predicting long-term shoreline response to climate change. *J. Geophys. Res. Earth Surf.* 122:782–806
- Voinov AA, DeLuca C, Hood RR, Peckham S, Sherwood CR, Syvitski JPM. 2010. A community approach to Earth systems modeling. *Eos Trans. AGU* 91:117–18
- Vousdoukas MI, Ferreira Ó, Almeida LP, Pacheco A. 2012. Toward reliable storm-hazard forecasts: XBeach calibration and its potential application in an operational early-warning system. *Ocean Dyn.* 62:1001–15
- Walstra DJR, Hoekstra R, Tonnon PK, Ruessink BG. 2013. Input reduction for long-term morphodynamic simulations in wave-dominated coastal settings. *Coast. Eng.* 77:57–70
- Walstra DJR, Mocke GP, Smit F. 1996. Roller contributions as inferred from inverse modelling techniques. *Coast. Eng. Proc.* 25:1205–18
- Wamsley TV, Cialone MA, Smith JM, Atkinson JH, Rosati JD. 2010. The potential of wetlands in reducing storm surge. *Ocean Eng.* 37:59–68
- Wandres M, Wijeratne EMS, Cosoli S, Pattiaratchi C. 2017. The effect of the Leeuwin Current on offshore surface gravity waves in southwest Western Australia. *J. Geophys. Res. Oceans* 122:9047–67
- Warner JC, Armstrong B, He R, Zambon JB. 2010. Development of a Coupled Ocean–Atmosphere–Wave–Sediment Transport (COAWST) modeling system. *Ocean Model.* 35:230–44
- Warner JC, Butman B, Dalyander PS. 2008a. Storm-driven sediment transport in Massachusetts Bay. *Cont. Shelf Res.* 28:257–82
- Warner JC, Defne Z, Haas K, Arango HG. 2013. A wetting and drying scheme for ROMS. *Comput. Geosci.* 58:54–61
- Warner JC, Sherwood CR, Signell RP, Harris CK, Arango HG. 2008b. Development of a three-dimensional, regional, coupled wave, current, and sediment-transport model. *Comput. Geosci.* 34:1284–306
- Warren IR, Bach HK. 1992. MIKE 21: a modelling system for estuaries, coastal waters and seas. *Environ. Softw.* 7:229–40
- Whitehead JC. 2003. One million dollars per mile? The opportunity costs of hurricane evacuation. *Ocean Coast. Manag.* 46:1069–83
- Williams WW. 1947. The determination of gradients on enemy-held beaches. *Geogr. J.* 109:76–90
- Wilson GW, Berezhnoy S. 2018. Surfzone state estimation, with applications to quadcopter-based remote sensing data. *J. Atmos. Ocean. Technol.* 35:1881–96
- Wilson GW, Özkan-Haller HT, Holman RA. 2010. Data assimilation and bathymetric inversion in a two-dimensional horizontal surf zone model. *J. Geophys. Res. Oceans* 115:C12057
- Wilson GW, Özkan-Haller HT, Holman RA, Haller MC, Honegger DA, Chickadel CC. 2014. Surf zone bathymetry and circulation predictions via data assimilation of remote sensing observations. *J. Geophys. Res. Oceans* 119:1993–2016
- Wu L, Chen C, Guo P, Shi M, Qi J, Ge J. 2011. A FVCOM-based unstructured grid wave, current, sediment transport model, I. Model description and validation. *J. Ocean Univ. China* 10:1–8
- Yates ML, Guza RT, O’Reilly WC. 2009. Equilibrium shoreline response: observations and modeling. *J. Geophys. Res.* 114:C09014

- Yates ML, Guza RT, O'Reilly WC, Hansen JE, Barnard PL. 2011. Equilibrium shoreline response of a high wave energy beach. *J. Geophys. Res. Oceans* 116:C04014
- Yin D, Xue ZG, Gochis DJ, Yu W, Morales M, Rafieeiniasab A. 2020. A process-based, fully distributed soil erosion and sediment transport model for WRF-Hydro. *Water* 12:1840
- Zambon JB, He R, Warner JC. 2014. Investigation of Hurricane Ivan using the coupled ocean–atmosphere–wave–sediment transport (COAWST) model. *Ocean Dyn.* 64:1535–54
- Zijlema M, Stelling G, Smit P. 2011. SWASH: an operational public domain code for simulating wave fields and rapidly varied flows in coastal waters. *Coast. Eng.* 58:992–1012



Contents

The Goldilocks Principle: A Unifying Perspective on Biochemical Adaptation to Abiotic Stressors in the Sea <i>George N. Somero</i>	1
Physiological Consequences of Oceanic Environmental Variation: Life from a Pelagic Organism's Perspective <i>Mark W. Denny and W. Wesley Dowd</i>	25
The Balance of Nature: A Global Marine Perspective <i>Constantin W. Arnscheidt and Daniel H. Rothman</i>	49
Ecological Leverage Points: Species Interactions Amplify the Physiological Effects of Global Environmental Change in the Ocean <i>Kristy J. Kroeker and Eric Sanford</i>	75
The Biological Effects of Pharmaceuticals in the Marine Environment <i>Marica Mezzelani and Francesco Regoli</i>	105
The Functional and Ecological Significance of Deep Diving by Large Marine Predators <i>Camrin D. Braun, Martin C. Arostegui, Simon R. Thorrold, Yannis P. Papastamatiou, Peter Gaube, Jorge Fontes, and Pedro Afonso</i>	129
Environmental DNA Metabarcoding: A Novel Method for Biodiversity Monitoring of Marine Fish Communities <i>Masaki Miya</i>	161
The Enzymology of Ocean Global Change <i>David A. Hutchins and Sergio A. Sañudo-Wilhelmy</i>	187
Using Chlorophyll Fluorescence to Determine the Fate of Photons Absorbed by Phytoplankton in the World's Oceans <i>Maxim Y. Gorbunov and Paul G. Falkowski</i>	213
Temporal and Spatial Signaling Mediating the Balance of the Plankton Microbiome <i>Yun Deng, Marine Vallet, and Georg Pohnert</i>	239
The Physiology and Biogeochemistry of SUP05 <i>Robert M. Morris and Rachel L. Spietz</i>	261

Machine Learning for the Study of Plankton and Marine Snow from Images <i>Jean-Olivier Irisson, Sakina-Dorothee Ayata, Dbugal J. Lindsay, Lee Karp-Boss, and Lars Stemmann</i>	277
Earth, Wind, Fire, and Pollution: Aerosol Nutrient Sources and Impacts on Ocean Biogeochemistry <i>Douglas S. Hamilton, Morgane M.G. Perron, Tami C. Bond, Andrew R. Bowie, Rebecca R. Buchholz, Cecile Guieu, Akinori Ito, Willy Maenhaut, Stelios Myriokefalitakis, Nazlı Olgun, Sagar D. Rathod, Kerstin Schepanski, Alessandro Tagliabue, Robert Wagner, and Natalie M. Mahowald</i>	303
The History of Ocean Oxygenation <i>Christopher T. Reinhard and Noah J. Planavsky</i>	331
Organic Matter Supply and Utilization in Oxygen Minimum Zones <i>Anja Engel, Rainer Kiko, and Marcus Dengler</i>	355
Argo—Two Decades: Global Oceanography, Revolutionized <i>Gregory C. Johnson, Shigeki Hosoda, Steven R. Jayne, Peter R. Oke, Stephen C. Riser, Dean Roemmich, Tobsio Suga, Virginie Thierry, Susan E. Wijffels, and Jianping Xu</i>	379
Ventilation of the Southern Ocean Pycnocline <i>Adele K. Morrison, Darryn W. Waugh, Andrew McC. Hogg, Daniel C. Jones, and Ryan P. Abernathy</i>	405
Aquatic Eddy Covariance: The Method and Its Contributions to Defining Oxygen and Carbon Fluxes in Marine Environments <i>Peter Berg, Markus Huettel, Ronnie N. Glud, Clare E. Reimers, and Karl M. Attard</i>	431
Modeling the Morphodynamics of Coastal Responses to Extreme Events: What Shape Are We In? <i>Christopher R. Sherwood, Ap van Dongeren, James Doyle, Christie A. Hegermiller, Tian-Jian Hsu, Tarandeep S. Kalra, Maitane Olabarrieta, Allison M. Penko, Yasbar Rafati, Dano Roelvink, Marlies van der Lugt, Jay Veeramony, and John C. Warner</i>	457

Errata

An online log of corrections to *Annual Review of Marine Science* articles may be found at <http://www.annualreviews.org/errata/marine>